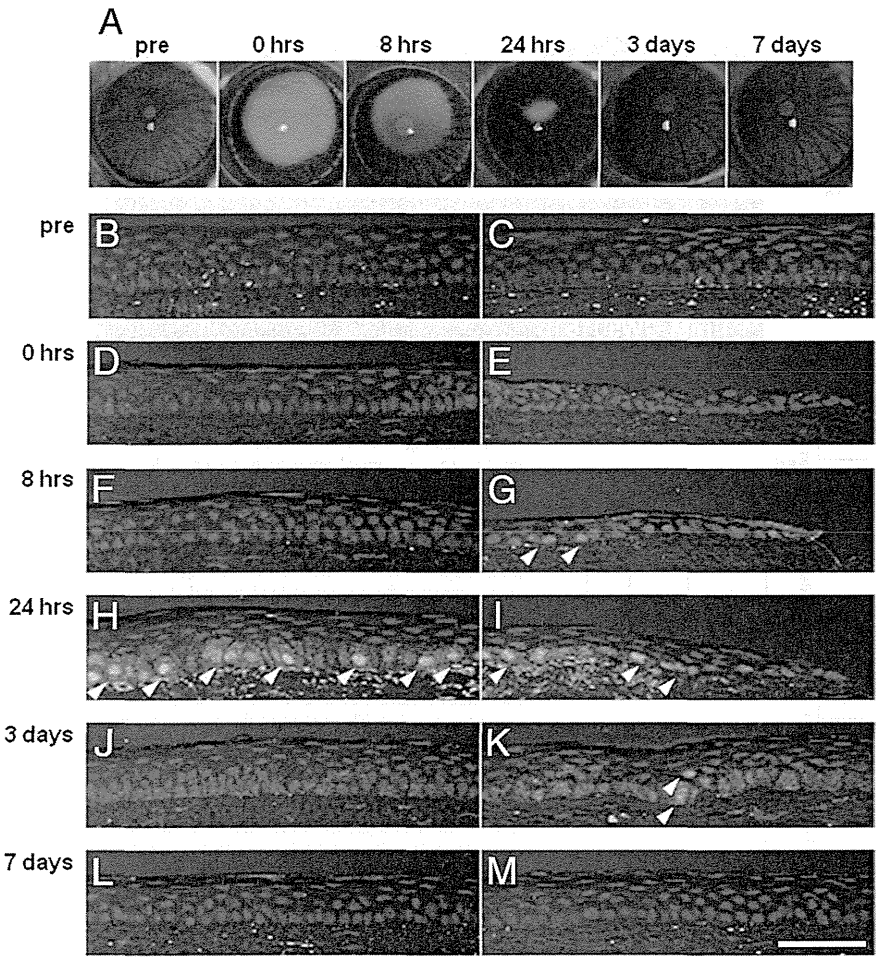

Figure 1. Protein expression of PPARδ in the rat corneal epithelia during wound healing. **A:** Representative photographs of the rats' ocular surfaces during corneal epithelial wound healing. Green areas represent fluorescein-stained areas of the corneal epithelial wounds. The wounds became increasingly smaller for up to 24 hours after wound generation and had completely healed at 3 days after the generation. **B–M:** Representative photographs of immunofluorescent staining for PPARδ in the rat corneal epithelia during wound healing. **B:** Corneal periphery before wound generation. **C:** Central cornea before wound generation. **D:** Corneal periphery immediately after wound generation. **E:** Edge of the epithelial wound immediately after wound generation. **F:** Corneal periphery at 8 hours after wound generation. **G:** Edge of the epithelial wound at 8 hours after wound generation. **H:** Area next to the epithelial wound edge at 24 hours after wound generation. **I:** Edge of the epithelial wound at 24 hours after wound generation. **J:** Corneal periphery at 3 days after wound generation. **K:** Central cornea at 3 days after wound generation. **L:** Corneal periphery at 7 days after wound generation. **M:** Central cornea at 7 days after wound generation. The blue and green staining represents the cellular nuclei and PPARδ, respectively. Staining of PPARδ is indicated by **white arrowheads** (**G–I** and **K**). PPARδ was faintly expressed at 8 and 24 hours after wound generation, peaking at 24 hours after wound generation. Scale bar = 50 μm.

ing the Cell Death Detection enzyme-linked immunosorbent assay (ELISA) (Roche Diagnostics) and the Cell Proliferation ELISA, BrdU (colorimetric) (Roche Diagnostics), respectively; their culture media were used for an evaluation of their LDH release using the LDH Cytotoxicity Detection Kit (Takara Bio, Shiga, Japan), according to manufacturers' protocols. The measured value in each culture well was then converted into a percentage when the averaged value of the nontreated group was 100% in each assay (at least 6 in each group of every assay).

Statistical Analyses

Statistical analyses were performed using the SPSS 11.0J data analysis system (SPSS Inc., Tokyo, Japan). The measured data in this study were statistically analyzed by using the Student's *t*-test, and $P < 0.05$ was considered statistically significant.

Results

Temporal Expression of PPARδ during Corneal Epithelial Wound Healing

Corneal epithelial wounds generated by surgical ablation in the rats were nearly completely healed at 24 hours and were completely healed at 3 days after generation (Figure 1A). During the wound-healing processes, an obvious sign of PPARδ immunostaining was not found on the nucleus of the corneal epithelial cells in the nonabraded corneal tissues or in the corneal tissues collected immediately after the ablations (Figure 1, B–M). Although some fine signals were observed in the corneal epithelia collected before wound generation (Figure 1, B and C), they were judged to be artifacts of the staining because they were observed in corneal epithelia and in the stroma, not corresponding to the cellular nuclei. However, a few faint signs of PPARδ immunostaining on the cell nucleus were observed at the region of the wound's edge of the corneal epithelia collected at 8 hours after the ablations (Figure 1G). In the corneal epithelia collected at 24 hours after the ablations, PPARδ immunostaining was widely observed on the cell nucleus of cells mainly distributed near the wounded region (Figure 1, H and I). Although the remaining few PPARδ-immunostained cell nuclei were observed in the central, just-closed regions of the wounds of the corneal epithelia collected at 3 days after the ablations (Figure 1K), they had completely disappeared at 7 days after the ablations (Figure 1, L and M). The expressions of PPARδ were localized in the corneal epithelial basal cells.

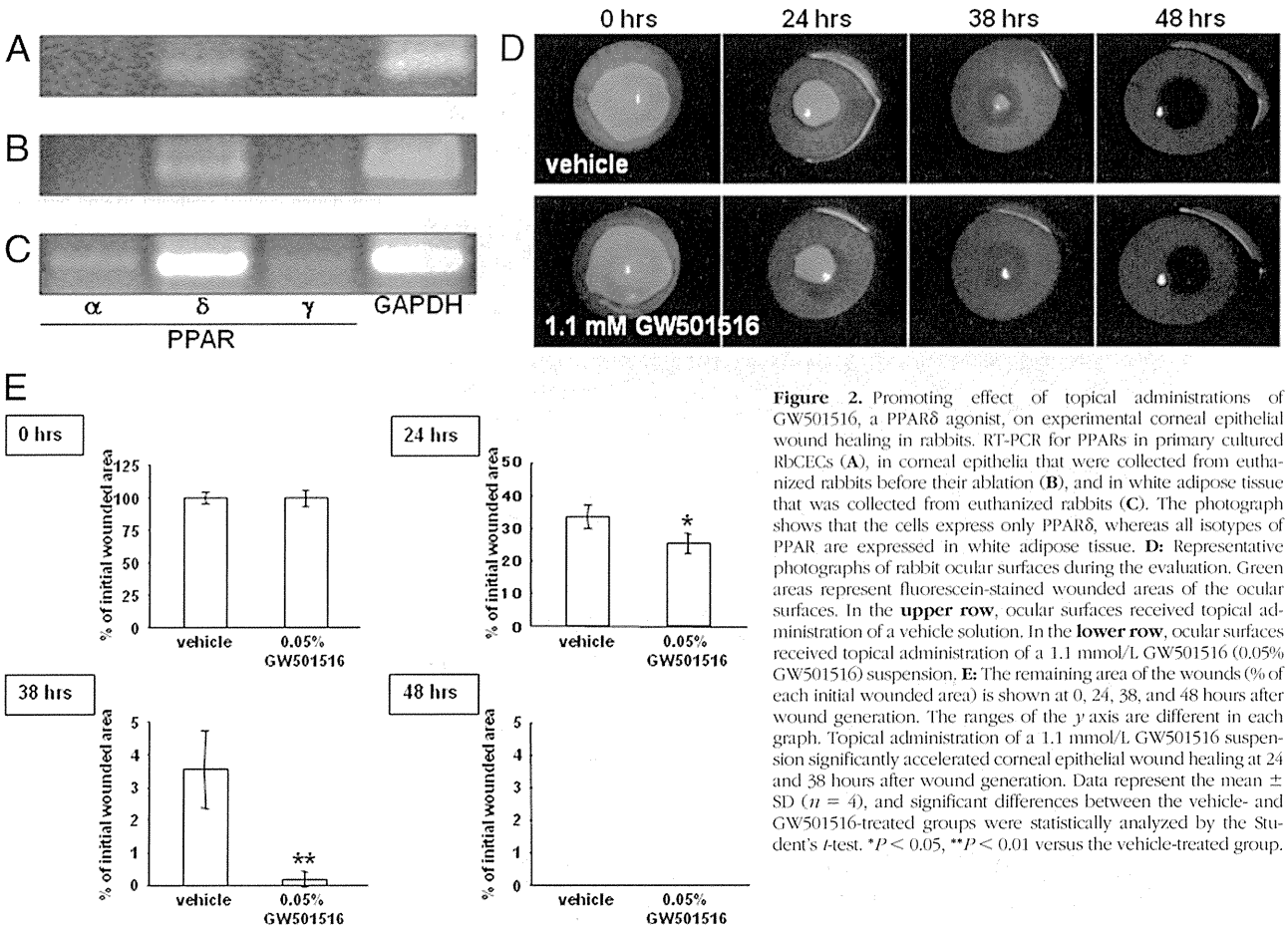

Figure 2. Promoting effect of topical administrations of GW501516, a PPARδ agonist, on experimental corneal epithelial wound healing in rabbits. RT-PCR for PPARs in primary cultured RbCECs (**A**), in corneal epithelia that were collected from euthanized rabbits before their ablation (**B**), and in white adipose tissue that was collected from euthanized rabbits (**C**). The photograph shows that the cells express only PPARδ, whereas all isotypes of PPAR are expressed in white adipose tissue. **D:** Representative photographs of rabbit ocular surfaces during the evaluation. Green areas represent fluorescein-stained wounded areas of the ocular surfaces. In the **upper row**, ocular surfaces received topical administration of a vehicle solution. In the **lower row**, ocular surfaces received topical administration of a 1.1 mmol/L GW501516 (0.05% GW501516) suspension. **E:** The remaining area of the wounds (% of each initial wounded area) is shown at 0, 24, 38, and 48 hours after wound generation. The ranges of the *y* axis are different in each graph. Topical administration of a 1.1 mmol/L GW501516 suspension significantly accelerated corneal epithelial wound healing at 24 and 38 hours after wound generation. Data represent the mean ± SD ($n = 4$), and significant differences between the vehicle- and GW501516-treated groups were statistically analyzed by the Student's *t*-test. $^{*}P < 0.05$, $^{**}P < 0.01$ versus the vehicle-treated group.

Effect of Topical Administrations of a PPARδ Agonist on Corneal Epithelial Wound Healing

To evaluate the effect of topical administrations of a PPARδ agonist on corneal epithelial wound healing, we first checked the expression of PPAR mRNAs in the rabbit corneal epithelia. Both cultured RbCECs (Figure 2A) and quiescent corneal epithelia that were collected before their ablation from rabbits (Figure 2B) expressed PPARδ mRNA, yet the expression of PPARα and PPARγ mRNAs was not detected in them. On the other hand, all isotypes of PPAR mRNAs were detected in white adipose tissue from rabbits (Figure 2C), demonstrating that the primers could detect PPARα and PPARγ mRNAs from rabbits, if they were expressed. Corneal epithelial wound healing of the wounds generated by surgical ablation in the rabbits significantly accelerated when treated by topical administrations of the PPARδ agonist (GW501516) suspension compared with the wounds that received the topical administration of a vehicle solution alone (Figure 2, D and E), both at 24 and 38 hours after wound generation. We evaluated the effect of another synthetic PPARδ agonist on corneal epithelial wound healing using the previously mentioned experimental model, in which the agonist also promoted the wound-healing processes, showing its dose dependency (data not shown).

Effect of a PPARδ Agonist on an in Vitro *Wound Closure System Using HCECs*

To demonstrate the specificity of a PPARδ agonist, GW501516, to PPARδ during corneal epithelial wound healing, we next evaluated it using an *in vitro* wound closure system, in which the cells were transfected with siRNAs for PPARδ to inhibit the expression, using HCECs. In cultured HCECs, PPARδ expression was significantly decreased by treatment with either one of two kinds of PPARδ siRNAs (S10883 or S10884), whereas the negative control (NC) siRNA did not show any decrease of the expression (Figure 3A). In this condition, we evaluated the effect of a PPARδ agonist, GW501516, on *in vitro* wound closure by HCECs. When the HCECs did not receive any siRNAs or received treatment of an NC siRNA, GW501516 showed significant promotion of the wound closure. On the other hand, when the cells received treatment of PPARδ siRNAs, in which PPARδ expression decreased, the agonist failed to demonstrate the promoting effect (Figure 3C). In addition, significant delays of the wound closure were also observed in the cells treated with PPARδ siRNAs (Figure 3, B and C). These findings suggested that the effect of a PPARδ agonist, GW501516, on corneal epithelial wound healing must be specifically demonstrated via PPARδ.

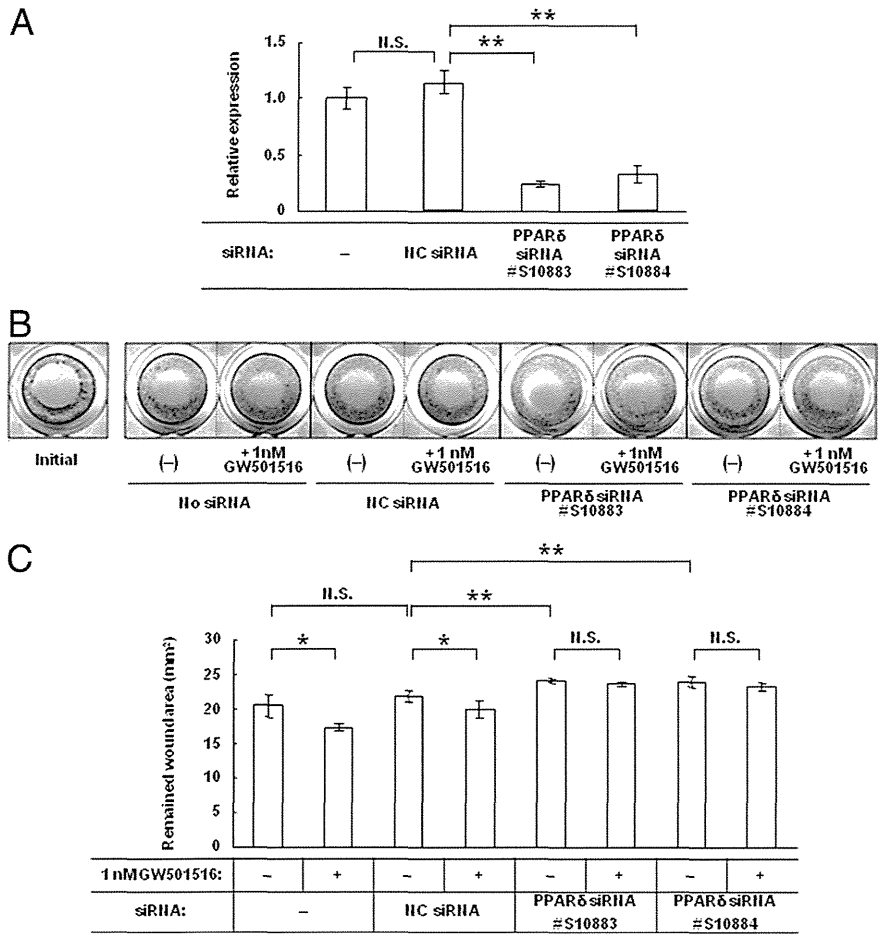

Figure 3. Promoting effect of GW501516, a PPARδ agonist, on *in vitro* corneal epithelial wound closure by HCECs and its specificity to PPARδ using PPARδ siRNAs during the processes. **A:** Real-time PCR for PPARδ shows that treatment of HCECs with siRNAs for PPARδ decreases the expression of PPARδ. Data represent the mean ± SD (n = 3 to 4). The significant differences between the no siRNA and NC siRNA treated groups was statistically analyzed by using the Student's t-test, in which there were no significant differences (N.S. indicates not significant), and among NC siRNA and PPARδ siRNA, treated groups were analyzed by using the Dunnett's test. $^{**}P < 0.01$ versus the NC siRNA-treated group. **B:** Representative photographs of experimental wells, in which stained HCECs are violet. Initial means the cells were stained immediately after the experimental wounds' generation. Pretreatment with a PPARδ agonist of the cells shows 1 nmol/L GW501516 or (–), which indicates no pretreatment. The transfected siRNAs are indicated as No siRNA, NC siRNA, PPARδ siRNA S10883, or PPARδ siRNA S10884. **C:** A graph showing each remaining wound area at 48 hours after wound generation. Data represent the mean ± SD (n = 4). The significant differences between the no siRNA and NC siRNA treated groups were statistically analyzed by using the Student's t-test, in which there were no significant differences, and those among NC siRNA and PPARδ siRNA treated groups were analyzed by using the Dunnett's test. $^{**}P < 0.01$ versus the NC siRNA treated group. The promoting effect of GW501516 on the wound closure processes was statistically analyzed by using the Student's t-test between groups that received the same siRNA treatments. $^{*}P < 0.05$.

Effect of a PPARδ Agonist on Inflammation-Induced HCEC Apoptosis

To elucidate the underlying mechanisms by which a PPARδ agonist promotes wound healing in corneal epithelia, we evaluated the effect of the PPARδ agonist, GW501516, on apoptosis, necrosis, and proliferation of cultured HCECs, which expressed all three PPAR mRNAs (Figure 4A). We theorize that the reason why the expression pattern of the isotype in the HCECs was not the same pattern as that observed in RbCECs (Figure 2, A and B) may be due to the differences between the species and the different function of those isotypes during corneal epithelial wound-healing processes among animal species. Because of the fact that the corneal epithelial wound-healing process at the ocular surface sometimes coincides with inflammation in both rat and rabbit experimental models *in vivo*, the cells were treated with cytokines (100 ng/mL TNF-α plus 10 ng/mL IFN-γ) to cause changes in cell viability. The treatment with cytokines caused an up-regulation of the PPARδ protein in the HCECs (Figure 4B), and this up-regulation agreed with the previous results observed in rats by using immunofluorescent microscopy (Figure 1, B–L). Moreover, the treatment with cytokines caused statistically significant increases of DNA fragmentation (Figure 5A) and LDH release (Figure 5C), as well as a decrease of BrdU incorporation (Figure 5D), in the HCECs. In these assay systems, treatment of the cells with camptothecin, a well-known topoisomerase I inhibitor and apoptosis inducer, produced a marked increase of DNA fragmentation (Figure 5A) and LDH release (Figure 5C), suggesting that the inhibitor caused apoptosis and necrosis of the cells. On the other hand, treatment of the cells with brain and reproductive organ-expressed (BRE) and EGF caused an obvious increase of BrdU incorporation (Figure 5D), suggesting that the supplemental treatment with BRE and EGF increased the proliferative activity of the cells.

In the previously mentioned assay systems, the PPARδ agonist, GW501516, caused a statistically significant inhibitory effect on the DNA fragmentation in the HCECs induced by treatment with cytokines (Figure 5A), suggesting that PPARδ agonists produce an anti-apoptotic effect. Although the effective concentrations of GW501516 in this study were low (1 nmol/L) compared with those in other reports, the EC_{50} value used in this study is similar to that used in the previous reports (1.1 nmol/L).[27] On the other hand, in the absence of cytokines, the DNA fragmentation (apoptosis) was induced by the treatment with GW501516 (Figure 5A).

We believe that these contrary effects are interesting because they suggest the function of PPARδ agonists on corneal epithelial cells. We hypothesize that PPARδ ago-

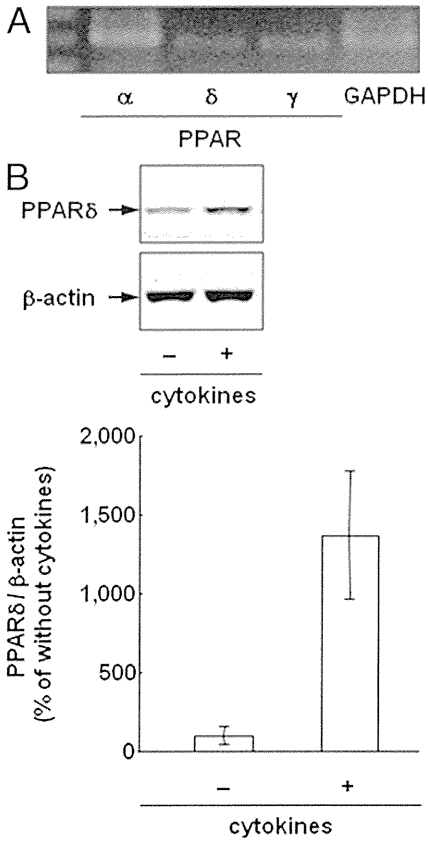

Figure 4. **A:** RT-PCR for PPARs in healthy HCECs. The human-derived cells expressed all PPARs: α, δ, and γ. GAPDH indicates glyceraldehyde-3-phosphate dehydrogenase. **B:** Western blot analysis for PPARδ as a target and β-actin as an internal standard. The results of the analyses show that the protein levels of PPARδ are up-regulated in the cells by treatment with cytokines (100 ng/mL TNF-α and 10 ng/mL IFN-γ). Data from Western blot analyses are represented as mean ± SD (n = 2).

nists may inhibit epithelial cell death when the cell death is ongoing; however, that cell death may be induced during active cell growth. In other words, PPARδ might have a function in maintaining the number of corneal epithelial cells. In fact, previously published studies have already demonstrated this contradiction. For example, one study[4] reported the anti-apoptotic effects of PPARδ, whereas another study[28] reported no anti-apoptotic effect and no proliferative effects of the receptor; a third study[29] reported the proliferative effects of the receptor. The findings of those studies have been reviewed in a separate publication,[30] in which the authors mention that those contradictory findings may be the result of the different experimental strategies used in the three previously referenced studies. In addition, they hypothesize that, although PPARδ affects the expression of inducers and inhibitors of cell proliferation, this receptor is not a bona fide cell cycle regulator with a defined function.[30] Our findings showed a novelty that a PPARδ agonist demonstrated such antithetic effects, even in a single evaluation system, one in which corneal epithelial cells were used. We are in the process of investigating this hypothesis. For example, although topical administrations of PPARδ agonists showed a promoting effect on corneal epithelial wound healing in rabbits, these compounds did not change the number of corneal cells when the animals did not receive corneal epithelial wounds (Y. Nakamura, unpublished data).

Furthermore, we also evaluated the effect of a PPARδ agonist/antagonist on early apoptosis in HCECs by using Western blot analysis for PARP, whose degradation suggests early apoptosis with activation of caspase. As a result, we observed that stimulation of the cells by cytokines induced marked degradation of PARP showing caspase activation and early apoptosis, but the degradation was inhibited by neither the agonist nor the antagonist (Figure 5B). These results suggest that PPARδ may

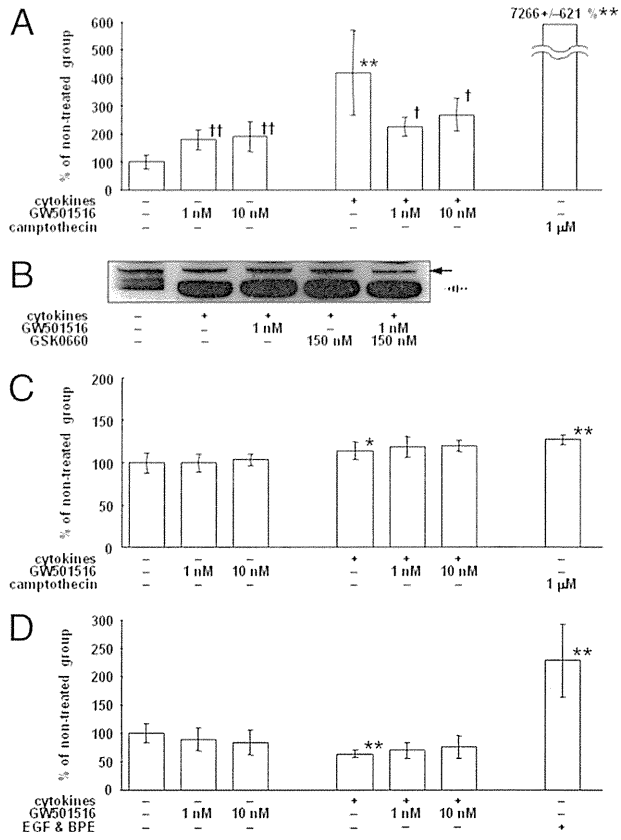

Figure 5. The effect of GW501516 on cytokine-induced DNA fragmentation (**A**), a representative photograph of Western blot analysis for PARP (**B**), LDH release (**C**), and decrease of BrdU incorporation (**D**), in healthy HCECs. In **A**, **C**, and **D**, levels are represented as a percentage of the nontreated group. Data in these three graphs are represented as mean ± SD (n = 12 for the nontreated group and the EGF- and bovine pituitary extract–treated groups, and n = 6 for the other groups), and significant differences between the nontreated group and the cytokine-treated group or each positive control group (1 μmol/L camptothecin-treated group for DNA fragmentation assay and LDH activity assay, and EGF- and bovine pituitary extract–treated group for BrdU incorporation assay) were statistically analyzed by the Student's t-test (*$P < 0.05$, **$P < 0.01$ versus the nontreated group). Significant differences between the nontreated group and GW501516-treated groups and between the cytokine-treated group and the cytokine plus GW501516-treated groups were analyzed by the Dunnett's test ($^{\dagger\dagger}P < 0.01$ versus the nontreated group, and $^{\dagger}P < 0.05$ versus the cytokine-treated group, respectively). In photographs of Western blot analysis for PARP (**B**), the **solid arrow** and the **dashed arrow** show intact PARP and degraded PARP, respectively. The photograph represents the result in three differently repeated experiments. Data show the degradation of PARP in cultured HCECs treated with cytokines and no effects of the PPARδ agonist/antagonist on the degradation.

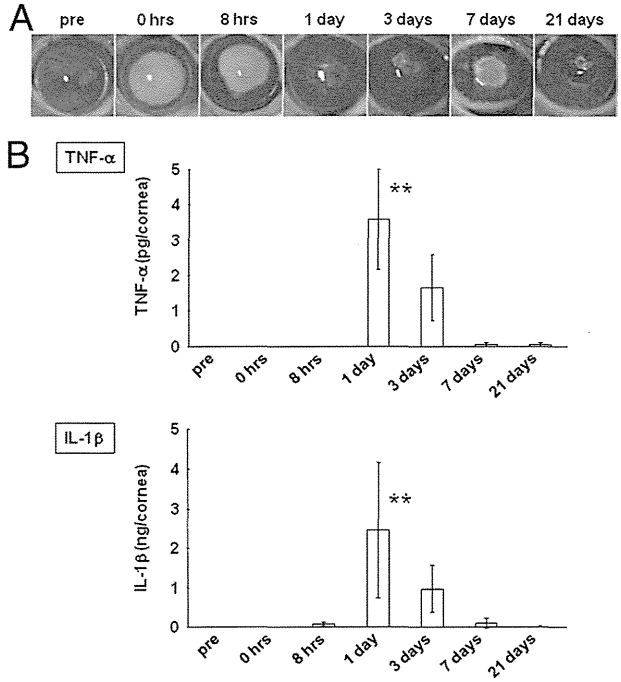

Figure 6. Analyses of the wound-healing process in rat corneas with alkali-induced keratitis. **A:** Representative photographs of rat ocular surfaces during corneal epithelial wound healing after receiving alkali attachment. Bright green areas represent fluorescein-stained areas of the corneal epithelial wounds. The wounds had healed by 1 to 3 days after injury, but recurrence of the wounds was observed in two of the three injured eyes. **B:** Protein expression changes of pro-inflammatory cytokines in corneas that received alkali-induced keratitis. Cytokines were measured by ELISA. **Top** and **bottom:** The levels of TNF-α and IL-1β, respectively. Data are represented as mean ± SD (n = 3), and significant differences in the corneal cytokine levels at each time point between the alkali attachment group and the nontreated group (pre) were statistically analyzed by the Dunnett's test. $^{**}P < 0.01$ versus the nontreated group.

not be affected in early apoptosis, at least not in our experiment.

In contrast to the results of the DNA fragmentation assay, GW501516 did not affect the LDH release from HCECs or the BrdU incorporation into those cells using the culture media, both in the absence and in the presence of cytokines, thus indicating that it is impossible for PPARδ agonists to inhibit cell necrosis, or promote cell proliferation, *in vitro*.

Sustained Expression of PPARδ and Corneal Epithelial Cell Death in Alkali-Induced Keratitis

Next, the investigation was focused on whether much inflammation at the ocular surface caused up-regulation of the PPARδ protein and the death of corneal epithelial cells. For this investigation, an alkali-induced keratitis rat model was used to observe healing processes of corneal epithelial wounds induced by alkali attachment; in some cases of this experimental keratitis model, we also observed their recurrence (Figure 6A). During those processes of this experimental keratitis, measurement by ELISA showed that the protein levels of cytokines TNF-α and IL-1β temporally increased in the rat corneas, with that increase peaking at 1 day after alkali attachment, and that the IL-1β level was much higher than the TNF-α level (Figure 6B). Although these data showed wide variances because the degree of corneal inflammation might be different among the animals, a statistically significant increase of corneal cytokines was observed at 1 day after their receipt of alkali attachment. The up-regulation of IL-1β was also observed by immunofluorescent microscopy. IL-1β staining of the cell nucleus was detected at 8 hours and at 1, 3, and 7 days after alkali attachment, and the signals were widely distributed throughout the corneal epithelia, thus showing an intense and temporal inflammatory response to alkali attachment (Figure 7, A–G). In addition, we assayed those cytokines secreted from isolated corneas, which had received alkali attachments before their enucleation, to their cultured media using an *ex vivo* tissue culture system to confirm that those cytokines were secreted from corneal epithelial cells that received alkali attachment. As a result, a significant increase of cytokines could not be observed (data not shown), although increases of cytokines in corneal epithelial cells had been observed after alkali attachment (Figure 7, A–G), thus supporting the ELISA data (Figure 6B). This difference may be explained by corneal inflammation increasing by interactions between corneal cells and other types of cells (eg, neutrophils),[31] whereas the infiltrations of kinds of inflammatory cells into the cornea were not permitted in this assay using an *ex vivo* system. Therefore, our data suggest that the inflammation with cytokine expression is induced after alkali attachment to the cornea and that at least some portion of cytokines is secreted from the corneal tissue; however, infiltrations of inflammatory cells into the cornea may be needed for an explosive increase of the cytokines. Similar to the corneal epithelial wound healing observed in rats after wound generation by surgical ablation, PPARδ was not observed in the corneal epithelial cells before and immediately after alkali attachment (Figure 7, H–K) and was up-regulated in the corneal epithelial cells of the corneas that received alkali attachment at the points of 8 hours and 1 and 7 days after the keratitis was induced (Figure 7, L–O, R, and S). Furthermore, the up-regulation of PPARδ disappeared at the points of 3 days showing its recurrent up-regulation (Figure 7, P–Q) and returned its initial level at 21 days (Figure 7, T–U). Thus, the period of up-regulation observed in the induced keratitis model was much longer than the period observed in the corneas that received surgical ablation (Figure 1, B–L), suggesting that sustained inflammation might cause a longer period of PPARδ up-regulation.

During the period of keratitis-associated inflammation, TUNEL-positive cells were detected in the corneal epithelia at 8 hours and at 1, 3, and 7 days after the alkali attachment (Figure 8, C–F), suggesting that the apoptotic cell death might be induced by the inflammation of the ocular surfaces in alkali-induced keratitis. On the other hand, TUNEL staining showed that the number of positive cells peaked at 8 hours after alkali attachment, whereas the peak of cytokine secretion was at 1 day. We theorize that this discrepancy (ie, the peak of TUNEL staining was after 8 hours when the cytokine levels only peaked after 1 day) may be

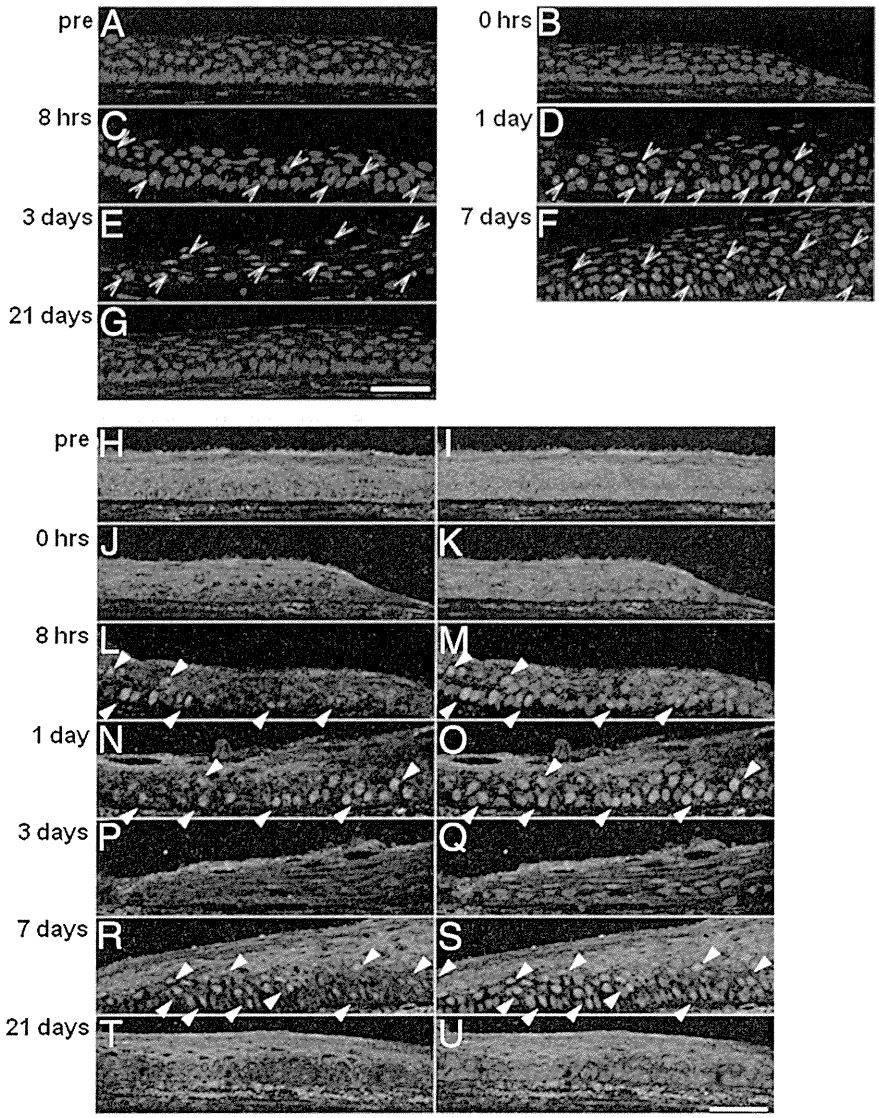

Figure 7. Analyses of the wound-healing process in rat corneas with alkali-induced keratitis (continued from Figure 6). Representative photographs of immunofluorescent staining for IL-1β showing before (**A**) or 0 hours (**B**), 8 hours (**C**), 1 day (**D**), 3 days (**E**), 7 days (**F**), or 21 days (**G**) after receiving alkali attachment in the rat corneal epithelia during wound healing. The blue and red staining represents the cellular nuclei and IL-1β, respectively, and typical staining of IL-1β is indicated by **open arrowheads**. IL-1β was expressed in cell nuclei at 8 hours and 1, 3, and 7 days after alkali attachment. Representative photographs of immunofluorescent staining for PPARδ showing before (**H** and **I**) or 0 hours (**J** and **K**), 8 hours (**L** and **M**), 1 day (**N** and **O**), 3 days (**P** and **Q**), 7 days (**R** and **S**), or 21 days (**T** and **U**) after the treatment, respectively, in the rat corneal epithelia during wound healing. The blue and green staining represents the cellular nuclei and PPARδ, respectively. Photographs **H**, **J**, **L**, **N**, **P**, **R**, and **T** and photographs **I**, **K**, **M**, **O**, **Q**, **S**, and **U** show immunofluorescent microscopy for PPARδ and those merged with DAPI staining, respectively. Typical staining of PPARδ is indicated by **closed arrowheads**, and PPARδ was obviously expressed in cell nuclei at 8 hours and 1 and 7 days after alkali attachment. Scale bar = 50 μm.

caused by apoptosis inducers, including other pro-inflammatory cytokines being secreted at 8 hours into the cornea, although they had not reached their peaks; then, they continuously induced apoptosis of the corneal epithelial cells from 8 hours until 21 days.

Temporal Expression of PPARδ in an ex Vivo *Human Corneal Epithelial Wound Model*

To elucidate the involvement of PPARδ in human corneal epithelial wound healing, we evaluated the expression of PPARδ in a human corneal epithelial wound model *ex vivo*. First, we demonstrated the expression of PPAR isoforms in human corneal epithelia obtained from healthy quiescent human corneal tissues immediately postmortem, and cDNA samples were separately prepared from their peripheral and central regions. PPAR α, δ, and γ mRNAs were detected in the peripheral region of the corneal epithelia, whereas only expressions of PPAR α and δ mRNAs were observed in the central region of them (Figure 9A). The corneal epithelial wounds generated by surgical ablation on the enucleated human corneoscleral tissues healed slowly, and re-epithelialization of those samples was incomplete, thus showing insufficient recovery of the cell layer after 48 hours of culture (Figure 9, F and G), which is in contrast to the *in vivo* experiment using an animal model (Figure 1). During such partial re-epithelialization processes *ex vivo*, the staining of PPARδ was not detected in the intact corneal epithelia before surgical ablation or in the corneal epithelia immediately and at 24 hours of culture after the generation of the wounds. However, some PPARδ signals were observed on the nucleus of corneal epithelia cells cultured for 48 hours after the ablations (Figure 9, F and G).

Next, human corneoscleral tissues were used to investigate the effect of inflammation on PPARδ protein expression. After a 24-hour culture of the tissues in the presence of 10 ng/mL TNF-α, obvious PPARδ signals were detected in the corneal epithelia of those samples (Figure 9H). A 24-hour culture of the tissues in the absence of TNF-α also caused the expression of PPARδ in their cor-

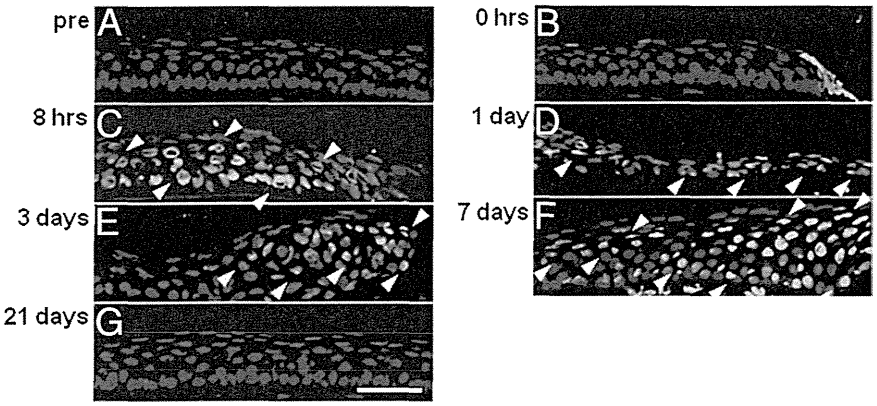

Figure 8. Analyses of the wound-healing process in rat corneas with alkali-induced keratitis (continued from Figure 7). Representative photographs of TUNEL staining showing before (**A**) or 0 hours (**B**), 8 hours (**C**), 1 day (**D**), 3 days (**E**), 7 days (**F**), or 21 days (**G**) after receiving alkali attachment in the rat corneal epithelia during wound healing. The blue and green staining represents cellular nuclei and TUNEL-positive staining, respectively. Typical TUNEL-positive staining is indicated by **white arrowheads** and was observed on the cell nuclei at 8 hours and 1, 3, and 7 days after alkali attachment. Scale bar = 50 μm.

neal epithelia (Figure 9I), which was unexpected. However, the frequencies of staining seemed to be up-regulated in the cytokine-treated tissues compared with the nontreated tissues (Figure 9H). To confirm the up-regulation of PPARδ, we tried to evaluate the effect of cytokines on the expression of PPARδ using cultured HCECs *in vitro*. As a result, the marked up-regulation of PPARδ could be detected in the cells treated with the cytokines (Figure 9, J and K). On the other hand, TUNEL staining showed that the treatment with TNF-α clearly caused DNA fragmentations, thus suggesting that the cytokine induced the cell apoptosis (Figure 9M).

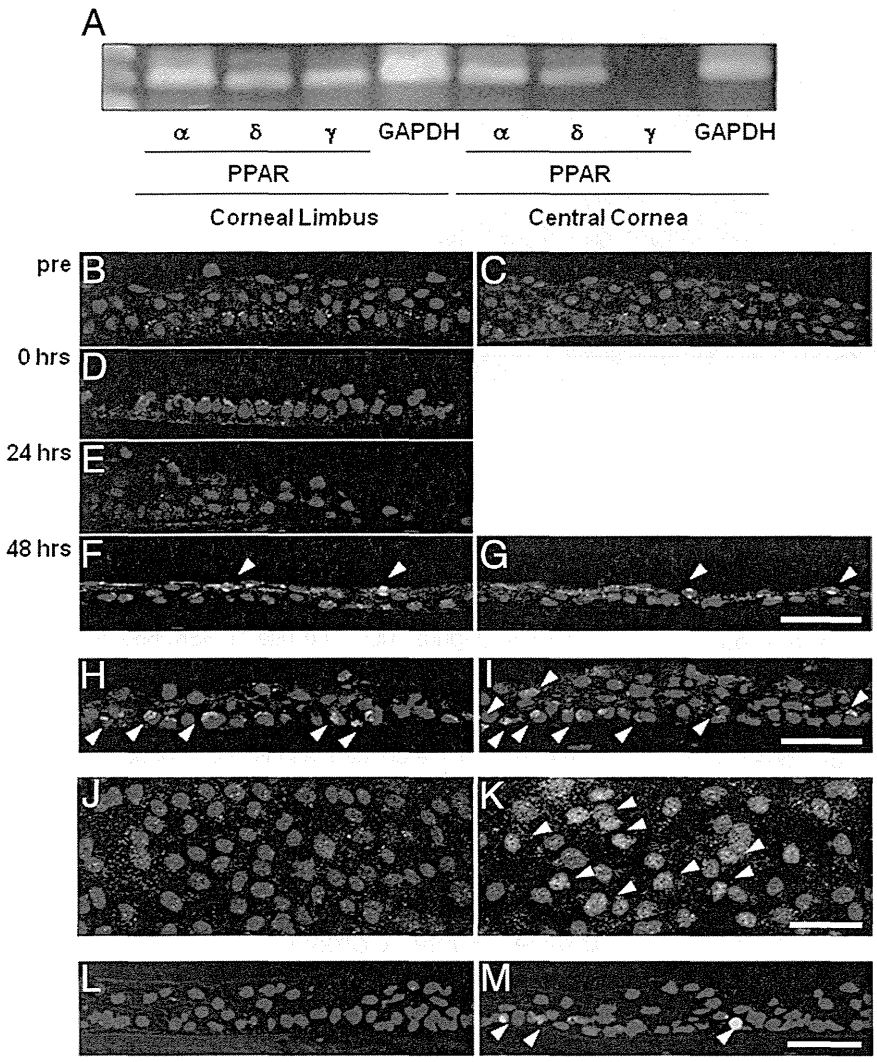

Figure 9. A: RT-PCR for PPARs in human corneal epithelial tissue using total RNAs separately prepared from the limbus and central region of the corneas. GAPDH indicates glyceraldehyde-3-phosphate dehydrogenase. **B–G:** Representative photographs of immunofluorescent staining for PPARδ in corneal epithelia on enucleated human corneoscleral samples during re-epithelialization *ex vivo* after mechanical abrasion. The blue and green staining represents the cell nuclei and PPARδ, respectively. Typical staining of PPARδ is indicated by **white arrowheads**. **B:** Corneal periphery before wound generation. **C:** Edge of the epithelial wound before wound generation. **D:** Edge of the epithelial wound immediately after wound generation. **E:** Edge of the epithelial wound at 24 hours after wound generation. **F:** Area next to the epithelial wound edge at 48 hours after wound generation. **G:** Edge of the epithelial wound at 48 hours after wound generation. In the abraded tissues incubated for 24 hours, the number of corneal epithelial cells was increased at the edge of the wounds, whereas PPARδ staining was not observed. On the other hand, limited, yet obvious, PPARδ staining was observed on the cell nuclei located at the peripheral region and the area next to the wound edge in the abraded tissues incubated for 48 hours. Scale bar = 50 μm. **H** and **I:** Representative photographs of immunofluorescent staining for PPARδ in corneal epithelia on enucleated human corneoscleral pieces during treatment without (**H**) or with (**I**) 10 ng/mL TNF-α *ex vivo*. The blue and green staining represents the cell nuclei and PPARδ, respectively. Typical staining of PPARδ is indicated by **white arrowheads**. Scale bar = 50 μm. **J** and **K:** Representative photographs of immunofluorescent staining for PPARδ in primary cultured HCECs during treatment without (**J**) or with (**K**) 20 ng/mL TNF-α *in vitro*. The blue and green staining represents the cell nuclei and PPARδ, respectively. Typical staining of PPARδ is indicated by **white arrowheads**. Scale bar = 50 μm. **L** and **M:** Representative photographs of TUNEL staining in corneal epithelia on enucleated human corneoscleral samples during treatment without (**L**) or with (**M**) 10 ng/mL TNF-α *ex vivo*. The blue and green staining represents the cell nuclei and TUNEL-positive staining, respectively. Typical TUNEL-positive staining is indicated by **white arrowheads** (**M**). Scale bar = 50 μm.

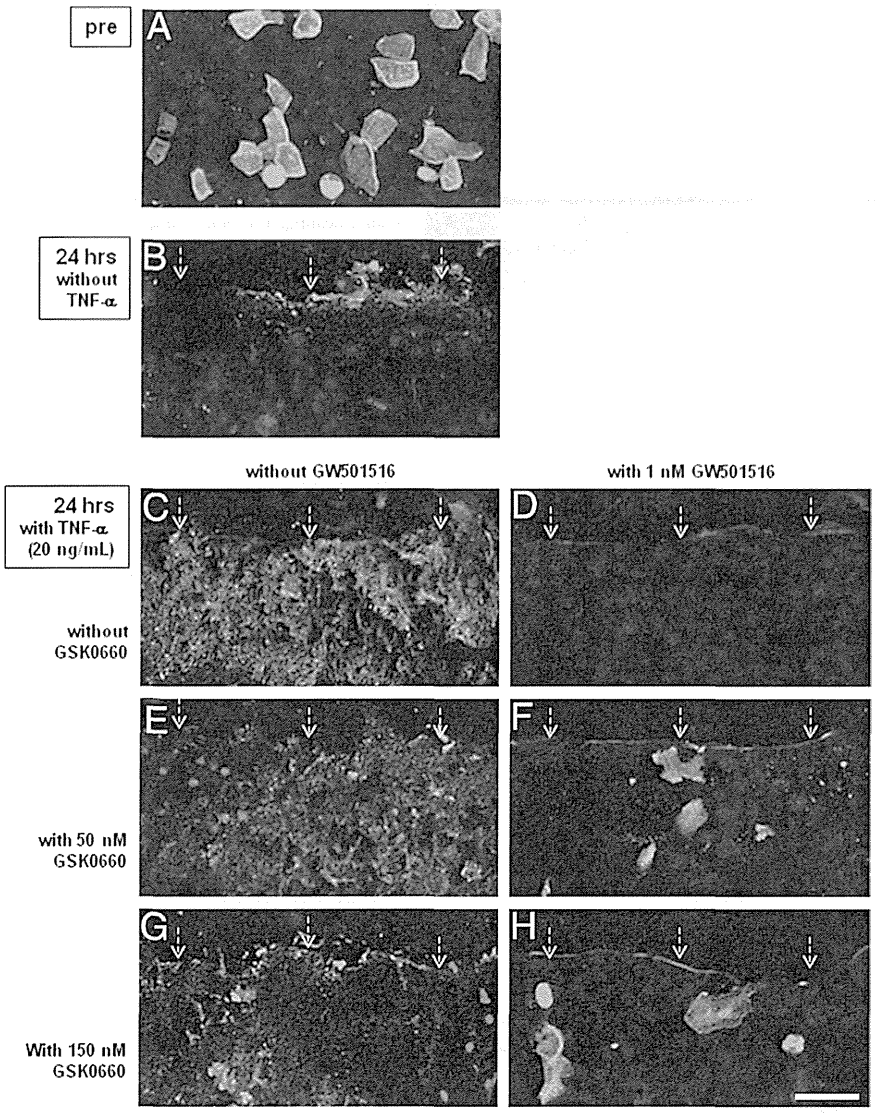

Figure 10. Representative photographs of immunofluorescent staining for annexin V in corneal epithelia on enucleated human corneoscleral samples during re-epithelialization *ex vivo* after mechanical abrasion. The green and red staining represents annexin V and the propidium iodide staining of cellular nuclei, respectively, and shows the cell death. The edges of corneal epithelial wounds are indicated by fine-dotted **white arrows** (**B**–**H**); the top side of each photograph is the center of the cornea, and the bottom side is the corneal limbus. The photographs show the corneal epithelia before wound generation (**A**), at 24 hours after wound generation with no additional treatments (**B**), at 24 hours after wound generation with stimulation by 20 ng/mL TNF-α (**C**), at 24 hours after wound generation with stimulation by 20 ng/mL TNF-α and pretreatment of 1 nmol/L GW501516 (**D**), at 24 hours after wound generation with stimulation by 20 ng/mL TNF-α and pretreatment of 50 nmol/L GSK0660 (**E**), at 24 hours after wound generation with stimulation by 20 ng/mL TNF-α and pretreatments of 50 nmol/L GSK0660 plus 1 nmol/L GW501516 (**F**), at 24 hours after wound generation with stimulation by 20 ng/mL TNF-α and pretreatment of 150 nmol/L GSK0660 (**G**), and at 24 hours after wound generation with stimulation by 20 ng/mL TNF-α and pretreatments of 150 nmol/L GSK0660 plus 1 nmol/L GW501516 (**H**). Scale bar = 50 μm.

Effect of a PPARδ Agonist on TNF-α–Induced HCEC Death in an ex Vivo *Model*

Because the inflammatory stimulation caused the up-regulation of PPARδ and DNA fragmentation of corneal epithelial cells, and because the PPARδ agonist, GW501516, could inhibit inflammatory cytokine-induced DNA fragmentation, we next evaluated the effect of GW501516 on TNF-α–induced corneal epithelial cell death using an *ex vivo* human corneoscleral tissue culture system (Figure 10). In this system, the cell death was detected as annexin V staining of their membranes and as propidium iodide staining of their nuclei. The corneal epithelial cell death was observed in noncultured corneoscleral tissues (Figure 10A), suggesting that the storage of the tissues for 4 to 5 days at 4°C caused them to die. After the 24-hour culture of the tissues, which had received surgical ablation of the corneal epithelia, cell death was observed only faintly at the edge of the corneal epithelial wound as annexin V staining (Figure 10B), thus showing a lower amount of cell death. However, when the tissues were treated with TNF-α, marked corneal epithelial cell death, which was observed as both annexin V– and propidium iodide–positive cells, was observed (Figure 10C). According to the results *in vitro* (Figure 5A), the TNF-α–induced corneal epithelial cell death was clearly inhibited by the pretreatment of those cells with the concentration of GW501516 (Figure 10D). The use of GSK0660, a specific PPARδ antagonist, did not exhibit anti-cell death effects (Figure 10, E and G). Interestingly, the effect of GW501516 on the TNF-α–induced cell death was partially inhibited by cotreatments of the concentrations of GSK0660 (Figure 10, F and H), thus showing, at least partially, the effect of GW501516 on cell death via PPARδ.

Particular Expression Pattern of PPARδ in Diseased Human Corneas

To investigate the particular expression pattern of PPARδ, diseased corneas, in which the corneal epithelial wounds were clearly observed by fluorescein testing (Figure 11,

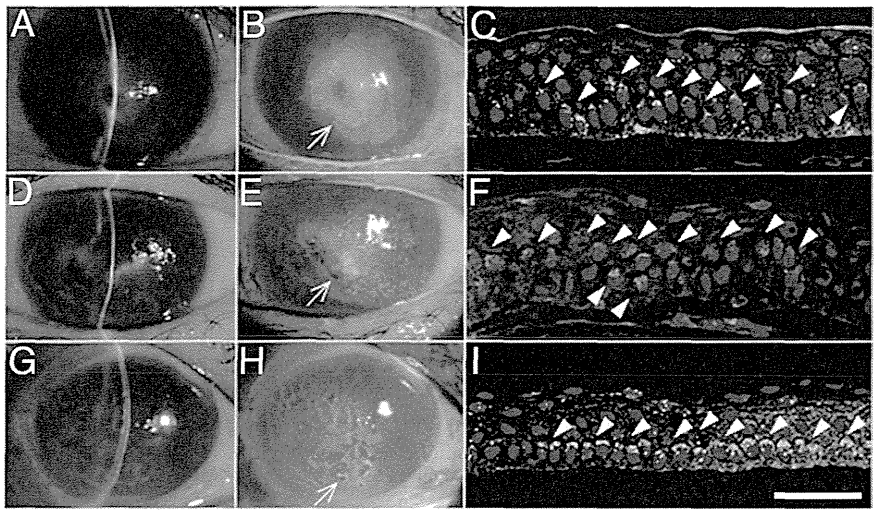

Figure 11. Expression of PPARδ in human corneal epithelia on enucleated corneal tissues. **A–F:** Corneas with herpetic keratitis. **G–I:** A cornea with luetic interstitial keratitis. The **left** (**A**, **D**, and **G**), **middle** (**B**, **E**, and **H**), and **right** (**C**, **F**, and **I**) column images show the ocular surfaces; corneal epithelial wounds are indicted by bright green fluorescein staining and immunofluorescent staining for PPARδ. Corneal epithelial wounds and the corneal staining of PPARδ are indicated by **white arrows** (**B**, **E**, and **H**) and by **white arrowheads** (**C**, **F**, and **I**), respectively. In the diseased corneas with corneal epithelial wounds, the marked expression of PPARδ was observed around the cell nuclei. Scale bar = 50 μm.

B, E, and H), were used in an attempt to detect PPARδ in corneal epithelia (Figure 11, C, F, and I). Healthy corneas did not express PPARδ proteins in their epithelial cells (Figure 9, B and C); however, the corneal epithelia obtained from herpetic keratitis corneas (Figure 11, C and F) and luetic interstitial keratitis corneas (Figure 11I) expressed PPARδ either on or nearby the cell nucleus.

Discussion

In this study, we demonstrated, for the first time to our knowledge, the following: i) a receptor PPARδ was temporally up-regulated during the corneal epithelial wound-healing processes, and the wound-healing process was clearly promoted by a PPARδ agonist; ii) PPARδ was up-regulated by stimulations with inflammatory cytokines, and a similar stimulation caused DNA fragmentation, which was inhibited by pretreatment with a PPARδ agonist in HCECs; iii) experimental ocular surface inflammation, induced by alkali attachment to the corneas, caused PPARδ up-regulation and DNA fragmentation in the associated corneal epithelial cells; iv) in an *ex vivo* experiment using human corneal tissue, PPARδ was up-regulated in the corneal epithelia during the re-epithelialization, treatment of those tissues by an inflammatory cytokine caused DNA fragmentation in the associated corneal epithelia, and the inflammatory stimulation-induced cell death of wounded corneal epithelia was inhibited by the treatment with a PPARδ agonist; and v) the up-regulation of PPARδ expression was observed in human diseased corneas with associated epithelial wounds. Furthermore, because the effect of a specific PPARδ agonist on inflammatory stimulation-induced corneal epithelial cell death in the *ex vivo* study was attenuated by the treatment with a specific PPARδ antagonist, this anti-cell death effect may, at least partially, be displayed via PPARδ. These findings clearly show that PPARδ plays an important role in corneal epithelial wound healing.

Our results suggest that ligand activation of PPARδ is involved in the wound healing of skin and in corneal epithelial wound healing. Previous studies have demonstrated the involvement of PPARδ in skin wound healing, as follows: i) PPARδ is temporally up-regulated during skin wound healing,[4] ii) the skin wound healing in *PPARδ*$^{+/-}$ mutant mice is delayed compared with *PPARδ*$^{+/+}$ mice,[4] and iii) i.p. administration of a PPARδ agonist promotes wound healing in the skin of mice.[12] In

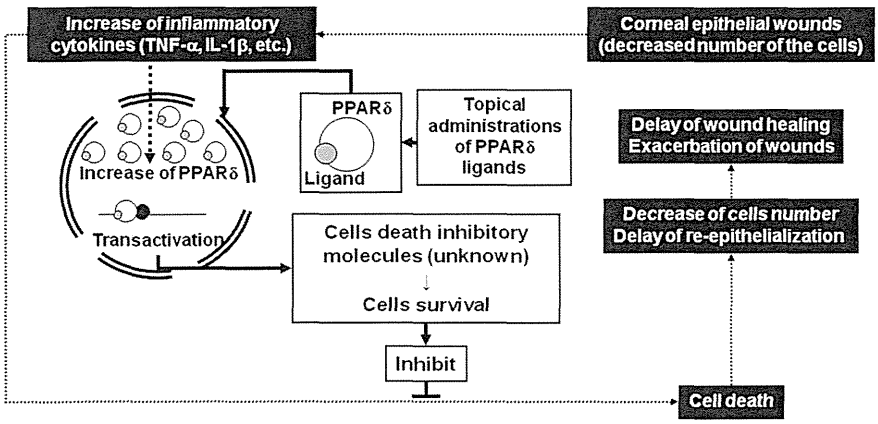

Figure 12. A schema of the proposed promoting effect of PPARδ agonists on corneal epithelial wound healing. Corneal epithelial wounds result in a decreased number of corneal epithelial cells and an increase of cytokines because of wound-associated inflammation. The cytokines induced cell death and up-regulation of PPARδ that results in an anti-apoptotic effect, even though the primary molecule responsible for that effect is unknown. Although the inflammation-induced cell death led to delayed wound healing and exacerbation of the wounds, those results can be inhibited by the activation of the PPARδ ligands.

addition, the findings of this study also demonstrated the temporal up-regulation of PPARδ during corneal epithelial wound healing and the promoting effect of the topical administration of a PPARδ agonist on corneal epithelial wound healing. Thus, we theorize that the topical administration of PPARδ agonists may possibly be a novel treatment for human diseases associated with corneal epithelial wounds.

The findings of this study also suggest that the mechanisms by which PPARδ agonists promote corneal epithelial wound healing may be through the inhibitory effects on cell death, because a PPARδ agonist inhibited cytokine-induced DNA fragmentation, apoptotic cell death in HCECs *in vitro*, and TNF-α–induced corneal epithelial cell death *ex vivo*. These findings are supported by some previous reports demonstrating the following: i) a PPARδ agonist shows the anti-apoptotic effect on skin wound healing[5,6]; ii) in this study, a PPARδ agonist could not change the level of BrdU incorporation into HCECs, suggesting that PPARδ agonists may not promote cell proliferation; and iii) the PPARδ antagonist, GSK0660, induced corneal epithelial cell migration, through both p38 mitogen-activated protein kinase activation and EGF receptor transactivation,[32] thus suggesting that PPARδ agonists may not induce corneal epithelial cell migration or proliferation. To date, we have been unable to identify the target genes that are responsible for the inhibitory effect of cell death regulated by the ligand activation of PPARδ in this study. Further studies are needed to elucidate how the ligand activation of PPARδ inhibits the death of HCECs.

Previous studies have reported that the inflammatory stimulation induces up-regulation of PPARδ and cell death in keratinocytes *in vitro*[13] and that the strong inflammation induced by alkali attachment to corneas causes the corneal epithelial defects and up-regulation of a variety of cytokines in mice.[33] These changes were also observed in this study using alkali attachment-induced experimental keratitis in rats; in addition to those changes previously reported, the TUNEL-positive staining in corneal epithelia was detected in the rats, suggesting the inflammation-induced cell death of corneal epithelia. Because some studies have already reported that the apoptosis of corneal epithelial cells is involved in corneal epithelial wounds,[34–36] we hypothesize that one of the mechanisms to promote corneal epithelial wound healing by PPARδ ligand activation may be to inhibit the inflammation-induced corneal epithelial cell death.

From those findings, we summarized the promoting effect of PPARδ agonists on corneal epithelial wound healing (Figure 12). The ocular surface inflammation that accompanies corneal epithelial wounds induces both the PPARδ up-regulation by which the corneal epithelial cells obtain a higher susceptibility to the ligands and the corneal epithelial cell death that causes delayed healing and exacerbation of the corneal epithelial wounds. However, the topical administrations of PPARδ agonists inhibited that cell death; as a result, the healing of those wounds was improved.

Interestingly, and similar to the results using experimental animals and cultured cells, the up-regulation of PPARδ was observed in the corneal epithelia of the human corneoscleral tissues during the re-epithelialization of those tissues after the surgical ablation *ex vivo*, and the inflammatory stimulation of the tissues using TNF-α caused corneal epithelial cell death, which was inhibited by treatment with a PPARδ agonist. These findings suggest that ligand activation of PPARδ may promote corneal epithelial wound healing in human eyes. Unexpectedly, cytokine treatment of human corneoscleral tissues in the *ex vivo* experiment did not result in the obvious up-regulation of PPARδ in corneal epithelia *ex vivo* (Figure 9, H and I), although we obtained the results that inflammatory cytokines could induce the up-regulation of PPARδ in experiments using HCECs *in vitro* (Figures 4B and 9, J and K). These discrepancies, observed in the results between the cultured tissues and the cultured cells, may be due to the different conditions of the corneal epithelial cells. In the *in vitro* systems, the nontreated cells had high cellular viabilities, whereas in the *ex vivo* system, viabilities of the cells on nontreated tissues depended on the tissue conditions. For example, in the *ex vivo* system, the cells on the tissues were at least partially undergoing the cell death processes before the culture (Figure 10A), possibly because of the storage of the corneal tissue samples at 4°C for several days. On the other hand, the nontreated cultured cells in the *in vitro* system did not show obvious cell death (data not shown). Therefore, the wounded corneal epithelial cells observed in the *ex vivo* system might be undergoing their wound-healing processes with up-regulation of PPARδ during their 24 hours of culture. Another reason why up-regulation of PPARδ was detected in the *ex vivo* system might be from unknown interactions that induce PPARδ up-regulation, between the corneal epithelial cells and the other types of cells (eg, corneal stromal cells or corneal endothelial cells) because the *ex vivo* system is unlike the *in vitro* system, in which only a single type of cells (ie, HCECs) exist. Moreover, the up-regulation of PPARδ was also observed in corneas obtained from patients with herpetic or luetic interstitial keratitis, two corneal diseases that are well-known for being accompanied by inflammation and epithelial wounds.

In conclusion, we demonstrated that PPARδ is clearly involved in corneal epithelial wound healing and that the wound-healing processes are promoted by PPARδ ligand activation, which inhibits the inflammation-induced corneal epithelial cell death. The promoting effect on corneal epithelial wound healing by PPARδ agonists may ultimately prove to be an effective method for the treatment of corneal epithelial wounds in human eyes in the clinical setting.

Acknowledgment

We thank John Bush for editing the manuscript.

References

1. Issemann I, Green S: Activation of a member of the steroid hormone receptor superfamily by peroxisome proliferators. Nature 1990, 347: 645–650

2. Dreyer C, Krey G, Keller H, Givel F, Helftenbein G, Wahli W: Control of the peroxisomal beta-oxidation pathway by a novel family of nuclear hormone receptors. Cell 1992, 68:879–887
3. Michalik L, Auwerx J, Berger JP, Chatterjee VK, Glass CK, Gonzalez FJ, Grimaldi PA, Kadowaki T, Lazar MA, O'Rahilly S, Palmer CN, Plutzky J, Reddy JK, Spiegelman BM, Staels B, Wahli W: International Union of Pharmacology, LXI: peroxisome proliferator-activated receptors. Pharmacol Rev 2006, 58:726–741
4. Michalik L, Desvergne B, Tan NS, Basu-Modak S, Escher P, Rieusset J, Peters JM, Kaya G, Gonzalez FJ, Zakany J, Metzger D, Chambon P, Duboule D, Wahli W: Impaired skin wound healing in peroxisome proliferator-activated receptor (PPAR)alpha and PPARbeta mutant mice. J Cell Biol 2001, 154:799–814
5. Di-Poï N, Tan NS, Michalik L, Wahli W, Desvergne B: Antiapoptotic role of PPARbeta in keratinocytes via transcriptional control of the Akt1 signaling pathway. Mol Cell 2002, 10:721–733
6. Di-Poï N, Michalik L, Tan NS, Desvergne B, Wahli W: The anti-apoptotic role of PPARbeta contributes to efficient skin wound healing. J *Steroid Biochem Mol Biol 2003, 85:257–265*
7. Tsuji K, Mitsutake S, Yokose U, Sugiura M, Kohama T, Igarashi Y: Role of ceramide kinase in peroxisome proliferator-activated receptor beta-induced cell survival of mouse keratinocytes. FEBS J 2008, 275: 3815–3826
8. Kim DJ, Bility MT, Billin AN, Willson TM, Gonzalez FJ, Peters JM: PPARbeta/delta selectively induces differentiation and inhibits cell proliferation. Cell Death Differ 2006, 13:53–60
9. Schmuth M, Haqq CM, Cairns WJ, Holder JC, Dorsam S, Chang S, Lau P, Fowler AJ, Chuang G, Moser AH, Brown BE, Mao-Qiang M, Uchida Y, Schoonjans K, Auwerx J, Chambon P, Willson TM, Elias PM, Feingold KR: Peroxisome proliferator-activated receptor (PPAR)-beta/delta stimulates differentiation and lipid accumulation in keratinocytes. J Invest Dermatol 2004, 122:971–983
10. Man MQ, Barish GD, Schmuth M, Crumrine D, Barak Y, Chang S, Jiang Y, Evans RM, Elias PM, Feingold KR: Deficiency of PPARbeta/delta in the epidermis results in defective cutaneous permeability barrier homeostasis and increased inflammation. J Invest Dermatol 2008, 128:370–377
11. Tan NS, Icre G, Montagner A, Bordier-ten-Heggeler B, Wahli W, Michalik L: The nuclear hormone receptor peroxisome proliferator-activated receptor beta/delta potentiates cell chemotactism, polarization, and migration. Mol Cell Biol 2007, 27:7161–7175
12. Ham SA, Kim HJ, Kim HJ, Kang ES, Eun SY, Kim GH, Park MH, Woo IS, Kim HJ, Chang KC, Lee JH, Seo HG. PPARdelta promotes wound healing by up-regulating TGF-beta1-dependent or -independent expression of extracellular matrix proteins. J Cell Mol Med 2010, 14:1747–1759
13. Tan NS, Michalik L, Noy N, Yasmin R, Pacot C, Heim M, Flühmann B, Desvergne B, Wahli W: Critical roles of PPAR beta/delta in keratinocyte response to inflammation. Genes Dev 2001, 15:3263–3277
14. Pflugfelder SC, Maskin SL, Anderson B, Chodosh J, Holland EJ, De Paiva CS, Bartels SP, Micuda T, Proskin HM, Vogel R: A randomized, double-masked, placebo-controlled, multicenter comparison of loteprednol etabonate ophthalmic suspension, 0.5%, and placebo for treatment of keratoconjunctivitis sicca in patients with delayed tear clearance. Am J Ophthalmol 2004, 138:444–457
15. Gündüz K, Ozdemir O: Topical cyclosporin treatment of keratoconjunctivitis sicca in secondary Sjögren's syndrome. Acta Ophthalmol (Copenh) 1994, 72:438–442
16. El-Shazly AH, El-Gohary AA, El-Shazly LH, El-Hossary GG: Comparison between two cyclooxygenase inhibitors in an experimental dry eye model in albino rabbits. Acta Pharm 2008, 58:163–173
17. Urashima H, Okamoto T, Takeji Y, Shinohara H, Fujisawa S: Rebamipide increases the amount of mucin-like substances on the conjunctiva and cornea in the N-acetylcysteine-treated in vivo model. Cornea 2004, 23:613–619
18. Tauber J, Davitt WF, Bokosky JE, Nichols KK, Yerxa BR, Schaberg AE, LaVange LM, Mills-Wilson MC, Kellerman DJ: Double-masked, placebo-controlled safety and efficacy trial of diquafosol tetrasodium (INS365) ophthalmic solution for the treatment of dry eye. Cornea 2004, 23:784–792
19. Sullivan DA, Sullivan BD, Evans JE, Schirra F, Yamagami H, Liu M, Richards SM, Suzuki T, Schaumberg DA, Sullivan RM, Dana MR: Androgen deficiency, Meibomian gland dysfunction, and evaporative dry eye. Ann N Y Acad Sci 2002, 966:211–222
20. Schultz G, Chegini N, Grant M, Khaw P, MacKay S. Effects of growth factors on corneal wound healing. Acta Ophthalmol Suppl 1992, (202):60–66
21. Condon PI, McEwen CG, Wright M, Mackintosh G, Prescott RJ, McDonald C: Double blind, randomised, placebo controlled, crossover, multicentre study to determine the efficacy of a 0.1% (w/v) sodium hyaluronate solution (Fermavisc) in the treatment of dry eye syndrome. Br J Ophthalmol 1999, 83:1121–1124
22. Nishida T, Nakagawa S, Manabe R: Clinical evaluation of fibronectin eyedrops on epithelial disorders after herpetic keratitis. Ophthalmology 1985, 92:213–216
23. Sosne G, Qiu P, Kurpakus-Wheater M: Thymosin beta 4: a novel corneal wound healing and anti-inflammatory agent. Clin Ophthalmol 2007, 1:201–207
24. Cortina MS, HE J, Li N, Bazan NG, Bazan HE: Neuroprotectin D1 synthesis and corneal nerve regeneration after experimental surgery and treatment with PEDF plus DHA. Invest Ophthalmol Vis Sci 2010, 51:804–810
25. Yamada N, Matsuda R, Morishige N, Yanai R, Chikama TI, Nishida T, Ishimitsu T, Kamiya A: Open clinical study of eye-drops containing tetrapeptides derived from substance P and insulin-like growth factor-1 for treatment of persistent corneal epithelial defects associated with neurotrophic keratopathy. Br J Ophthalmol 2008, 92:896–900
26. Watanabe K, Nakagawa S, Nishida T: Chemotactic and haptotactic activities of fibronectin for cultured rabbit corneal epithelial cells. Invest Ophthalmol Vis Sci 1988, 29:572–577
27. Sznaidman ML, Haffner CD, Maloney PR, Fivush A, Chao E, Goreham D, Sierra ML, LeGrumelec C, Xu HE, Montana VG, Lambert MH, Willson TM, Oliver WR Jr, Sternbach DD. Novel selective small molecule agonists for peroxisome proliferator-activated receptor delta (PPARdelta): synthesis and biological activity. Bioorg Med Chem Lett 2003, 13:1517–1521
28. Burdick AD, Bility MT, Girroir EE, Billin AN, Willson TM, Gonzalez FJ, Peters JM: Ligand activation of peroxisome proliferator-activated receptor-beta/delta(PPARbeta/delta) inhibits cell growth of human N/TERT-1 keratinocytes. Cell Signal 2007, 19:1163–1171
29. Romanowska M, al Yacoub N, Seidel H, Donandt S, Gerken H, Phillip S, Haritonova N, Artuc M, Schweiger S, Sterry W, Foerster J: PPARdelta enhances keratinocyte proliferation in psoriasis and induces heparin-binding EGF-like growth factor. J Invest Dermatol 2008, 128:110–124
30. Müller R, Rieck M, Müller-Brüsselbach S: Regulation of cell proliferation and differentiation by PPARbeta/delta. PPAR Res 2008, 2008:614852
31. Li Q, Fukuda K, Lu Y, Nakamura Y, Chikama T, Kumagai N, Nishida T: Enhancement by neutrophils of collagen degradation by corneal fibroblasts. J Leukoc Biol 2003, 4:412–419
32. Zhang Z, Pan Z, Zhang F, Reinach PS. Pparβ antagonist mediates increases in human corneal epithelial cell migration through P38 Mapk activation. Assoc Res Vision Ophthalmol (ARVO) 2010, Program 1973/Poster D904
33. Sotozono C, He J, Matsumoto Y, Kita M, Imanishi J, Kinoshita S: Cytokine expression in the alkali-burned cornea. Curr Eye Res 1997, 16:670–676
34. Yeh S, Song XJ, Farley W, Li DQ, Stern ME, Pflugfelder SC: Apoptosis of ocular surface cells in experimentally induced dry eye. Invest Ophthalmol Vis Sci 2003, 44:124–129
35. Nakamura S, Shibuya M, Saito Y, Nakashima H, Saito F, Higuchi A, Tsubota K: Protective effect of D-beta-hydroxybutyrate on corneal epithelia in dry eye conditions through suppression of apoptosis. *Invest Ophthalmol Vis Sci 2003, 44:4682–4688*
36. Chen W, Zhang X, Zhang J, Chen J, Wang S, Wang Q, Qu J: A murine model of dry eye induced by an intelligently controlled environmental system. Invest Ophthalmol Vis Sci 2008, 49:1386–1391

Heat treatment of retinal pigment epithelium induces production of elastic lamina components and antiangiogenic activity

Eiichi Sekiyama,*,† Magali Saint-Geniez,*,† Kazuhito Yoneda,‖ Toshio Hisatomi,§ Shintaro Nakao,§ Tony E. Walshe,*,† Kazuichi Maruyama,*,‖ Ali Hafezi-Moghadam,§ Joan W. Miller,§ Shigeru Kinoshita,‖ and Patricia A. D'Amore*,†,‡,[1]

*Schepens Eye Research Institute, †Department of Ophthalmology, ‡Department of Pathology, and §Angiogenesis Laboratory, Massachusetts Eye and Ear Infirmary, Harvard Medical School, Boston, Massachusetts, USA; and ‖Department of Ophthalmology, Kyoto Prefectural University of Medicine, Graduate School of Medicine, Kyoto, Japan

ABSTRACT **Age-related macular degeneration (AMD) is the leading cause of blindness in the Western world. In advanced AMD, new vessels from choriocapillaris (CC) invade through the Bruch's membrane (BrM) into the retina, forming choroidal neovascularization (CNV). BrM, an elastic lamina that is located between the retinal pigment epithelium (RPE) and CC, is thought to act as a physical and functional barrier against CNV. The BrM of patients with early AMD are characterized by decreased levels of antiangiogenic factors, including endostatin, thrombospondin-1 (TSP-1), and pigment epithelium-derived factor (PEDF), as well as by degeneration of the elastic layer. Motivated by a previous report that heat increases elastin expression in human skin, we examined the effect of heat on human ARPE-19 cell production of BrM components. Heat treatment stimulated the production of BrM components, including TSP-1, PEDF, and tropoelastin *in vitro* and increased the antiangiogenic activity of RPE measured in a mouse corneal pocket assay. The effect of heat on experimental CNV was investigated by pretreating the retina with heat *via* infrared diode laser prior to the induction of CNV. Heat treatment blocked the development of experimental CNV *in vivo*. These findings suggest that heat treatment may restore BrM integrity and barrier function against new vessel growth.—Sekiyama, E., Saint-Geniez, M., Yoneda, K., Hisatomi, T., Nakao, S., Walshe, T. E., Maruyama, K., Hafezi-Moghadam, A., Miller, J. W., Kinoshita, S., D'Amore, P. A. Heat treatment of retinal pigment epithelium induces production of elastic lamina components and anti-angiogenic activity. *FASEB J.* 26, 567–575 (2012). www.fasebj.org**

Key Words: choroidal neovascularization · transpupillary thermotherapy · endostatin · thrombospondin-1 · elastin

AGE-RELATED MACULAR DEGENERATION (AMD), the leading cause of blindness in the elderly population in the Western world (1), is classified as either wet or dry type. In contrast to the patients with dry AMD, in whom impairment of vision is gradual, wet AMD has rapid and devastating visual effects. The clinical and histopathologic features of wet AMD involve the dysfunction of retinal pigment epithelium (RPE), Bruch's membrane (BrM) and the choriocapillaris (CC). In wet AMD, new vessels from the CC invade through the BrM into the retina, resulting in choroidal neovascularization (CNV). Early AMD is distinguished by subretinal deposits and atrophic changes in the RPE, which are not associated with changes in visual acuity. However, once new blood vessels develop and invade the retinal space, vision is lost. Thus, strategies that could prevent the progression to wet AMD would be valuable.

BrM, which is located between the RPE and CC, is composed of 5 distinct layers: a central elastic layer, bounded on both sides by collagenous layers, and bordered externally by the basal laminas of the RPE and CC. The basement membranes underlying the RPE and the CC endothelial cells contain collagen IV, laminin, and decorin. Many of these molecules have reported effects on the proliferation and/or survival of vascular endothelium. Collagen IV α 2 chain has been reported to induce apoptosis of vascular endothelial cells (2), and α 3 chain has been shown to inhibit the vascular endothelial proliferation and block tube formation *in vitro* (3). The collagenous layers of BrM include collagens I, III, and XVIII, and fibronectin. Collagen I is reported to down-regulate VEGF-mediated VEGFR2 activation (4) and to bind thrombospondin-1 (TSP-1), a major antiangiogenic factor (5). Through cleavage by enzymes, including cathepsin B and MMP-7, collagen XVIII produces endostatin, a well-described endogenous antiangiogenic factor, which has been shown to regulate CNV (6). The elastic layer, which is formed by the cross-linking of tropoelastin on microfibrils of fibrillin-1 and -2 molecules, is believed to

[1] Correspondence: Schepens Eye Research Institute, 20 Staniford St., Boston, MA 02114, USA. E-mail: patricia.damore@schepens.harvard.edu

doi: 10.1096/fj.11-184127

act as physical barrier against new vessel growth (7, 8). Interestingly, BrM from patients with early AMD has been reported to have decreased levels of antiangiogenic molecules, including endostatin, TSP-1, and pigment epithelium-derived factor (PEDF) (9–11), as well as degeneration of the elastic layer (8). Taken together, these observations indicate that the BrM functions as a physical and functional barrier against the growth of new blood vessel from the CC.

Previous reports have demonstrated that heat induces elastin expression in human skin (12) and that the expression of heat-shock protein (HSP) increases the levels of endostatin and TSP-1 in tumors (13). With a goal of identifying a means to restore BrM, we investigated the effect of mild heat treatment on human RPE-production of BrM components. In addition, we tested the effect of heat on the retina *in vivo* using topical heat treatment with an infrared diode laser (IDL). Results of these studies suggest that heat treatment can induce the expression of components of BrM and thus might be useful in preventing the progression to neovascular AMD.

MATERIALS AND METHODS

ARPE-19 cell cultures

ARPE-19 cells obtained from American Type Culture Collection (Manassas, VA, USA) were used between passages 21 and 25. Transwells (0.4-μm pore size, 12- or 24-mm diameter; Corning/Costar, Corning, NY, USA) were coated with laminin, and ARPE-19 cells ($\sim 1.7\times10^5$ cells/cm^2) were seeded in DMEM/F-12 culture medium, supplemented with 100 U/ml penicillin-streptomycin and 1% FBS. The medium was changed 2×/wk. Cells were cultured for ≥4 wk to form differentiated monolayers. RNAs were isolated from cells after 1, 2, 3, and 4 wk of culture.

For heat treatment, ARPE-19 cells grown for 4 wk on the transwells were cultured at 43°C for 30 min. RNA was isolated at 15 min and 1, 2, and 4 h after heat treatment, and cell-associated proteins were examined in cell lysates collected at 2 and 4 h after heat treatment. Proteins secreted into the culture medium were collected at 4 h after heat treatment and analyzed.

RNA isolation and real-time PCR analysis

Total RNA was extracted (RNAqueousTM-4PCR kit; Ambion, Austin, TX, USA), according to the manufacturer's instructions. Residual DNA was removed by treatment with 1 U DNase I (Ambion) at 37°C for 20 min. RNA (1 μg) was reverse-transcribed, and 1/20 of the total cDNA was used in each amplification reaction. Each gene was quantified [Prism 9700 Sequence Detection System; Applied Biosystems (ABI), Foster City, CA, USA] according to the manufacturer's instructions (**Table 1**). Reactions were performed in 25 μl with 0.3 μM primers and master mix (SYBR Green Master mix; ABI). PCR cycles consisted of an initial denaturation step at 95°C for 10 min, followed by 40 cycles at 95°C for 15 s and at 60°C for 60 s. To confirm amplification specificity, PCR products from each primer pair were subjected to a melting curve analysis. Amplification of the GAPDH was performed on each sample as a control for sample loading and to allow normalization between samples. Each sample was run in duplicate, and each experiment was conducted ≥3 times.

Western blot analysis

ARPE-19 cells were collected in lysis buffer (10 mM Tris-HCl, pH 7.4; 5 mM EDTA; 50 mM NaCl; 1% Triton X-100; 50 mM NaF; 1 mM phenylmethylsulfonyl fluoride; 2 mM Na_3VO_4; and 20 mg/ml aprotinin), and protein concentrations were quantified using the NanoDrop (Scrum, Tokyo, Japan). Medium conditioned by ARPE-19 cells was concentrated 10-fold with a centrifugal filter with a molecular size cutoff of 10 kDa (Amicon Ultra; Millipore, Bedford, MA, USA), and equal volumes of samples were analyzed. Proteins from cell lysates and conditioned medium were separated by SDS-PAGE. Cell lysates were probed with rabbit polyclonal anti-human tropoelastin (1:300; Elastin Products Co., Owensville, MO, USA) and mouse monoclonal anti-human TSP-1 (1:400; Abcam, Cambridge, MA, USA). Concentrated medium was probed with mouse monoclonal anti-human endostatin (1:100; Oncogene, San Diego, CA, USA) and mouse monoclonal anti-human PEDF (1:1000; Millipore). Binding was detected with the appropriate HRP-conjugated secondary antibody (1:1000; Amersham Biosciences, Piscataway, NJ, USA) and ECL-Plus Western blotting Detection System (GE Healthcare, Waukesha, WI, USA). The intensity of Western blot bands was quantified by densitometric analysis using NIH ImageJ (n=3; U.S. National Institutes of Health, Bethesda, MD, USA).

TUNEL assay

ARPE-19 cell apoptosis was evaluated using the *in situ* cell death detection kit (TMR red, Roche, Mannheim, Germany),

TABLE 1. *Primers used for real-time PCR*

Primer	Source	Catalog number
Collagen I	Qiagen (Valencia, CA, USA)	QT00037793
Collagen IV	Qiagen	QT00005250
Collagen XVIII	SABiosciences (Frederick, MD, USA)	PPH01141E-200
Decorin	SABiosciences	PPH01900A-200
Fibronectin	SABiosciences	PPH00413B-200
Laminin	SABiosciences	PPH20901E-200
Tropoelastin	SABiosciences	PPH06895E-200
Fibrillin-1	Qiagen	QT00024507
Thrombospondin-1	SABiosciences	PPH00799E-200
PEDF	SABiosciences	PPH00805A-200
Cathepsin B	Qiagen	QT00088641
MMP-7	Qiagen	QT00001456

according to the manufacturer's instructions. Briefly, cells were fixed with 4% paraformaldehyde for 1 h at room temperature and then permeabilized with 0.1% TritonX-100 in 0.1% sodium citrate for 2 min on ice. After the incubation with TUNEL reaction mixture and DAPI for 60 min at 37°C in the dark, cells were observed. Three wells were analyzed by counting apoptotic cells in 4 randomly chosen fields.

Transmission electron microscopy

Monolayers of ARPE-19 cells cultured on transwells for 3 d and 4 wk were fixed with half-strength Karnovsky's fixative, followed by 2% osmium tetroxide and stained en block with 0.5% uranyl acetate. After dehydration and embedding, ultrathin sections were visualized using a transmission electron microscope (Model 410; Phillips, Amsterdam, The Netherlands).

Effect of medium conditioned by heat-treated ARPE-19 cells on endothelial cell wound closure assay and proliferation

Medium was collected after 4 h of conditioning by heat-treated ARPE-19 cells; unconditioned medium served as a control. Medium was mixed with an equal volume of endothelial basal medium (EBM-2) supplemented with SingleQuots (Lonza, Walkersville, MD, USA), 20% FBS, and 1× glutamine-penicillin-streptomycin and tested for its effect on the closure of scratch wounds by human umbilical vein cells (HUVECs). Monolayers of confluent HUVECs in 24-well plates (Corning/Costar) were scratch wounded using the p1000 pipette tips. Two scratches/well were made (n=4). The progress of wound closure was photographed with an inverted microscope equipped with a digital camera (SPOT; Diagnostic Imaging, Sterling Heights, MI, USA) immediately after injury and at 16 h after wounding. The width of the wound was measured using NIH ImageJ software. Three random measurements were taken of each wound, and their average was taken as the width of each wound.

For the assay of proliferation, HUVECs were seeded at 2×10^4 cells/well in triplicates onto 12-well plates (Corning/Costar). After 3 d, cell proliferation was evaluated by direct cell count of trypsin-detached cells with a hemocytometer (n=3).

Corneal micropocket assay

Rodent studies were approved by the Animal Care Committee of the Massachusetts Eye and Ear Infirmary. BALB/c mice were anesthetized by intraperitoneal injection of ketamine at 100 mg/kg and xylazine at 10 mg/kg. Hydron pellets (0.3 μl) containing 200 ng of human VEGF (201-LB; R&D Systems, Minneapolis, MN, USA) were prepared. Heat-treated (n=6) or control untreated (n=10) ARPE-19 cells cultured on the transwells were dissected into 0.3-μm-square pieces and implanted into the corneas with VEGF-containing pellets. The pellets and tissues were positioned 1 mm from the corneal limbus, as described previously (14). Implanted eyes were treated topically with bacitracin ophthalmic ointment (E. Fougera & Co., Melville, NY, USA). At 6 d after implantation, digital images of the corneal vessels were obtained and recorded using OpenLab 2.2.5 software (Improvision Inc., Waltham, MA, USA) with standardized illumination and contrast. Quantification of neovascularization in the mouse corneas was performed using NIH ImageJ software.

Effect of elastin on endothelial cell migration

Transwells (3.0-μm pore size, 6.5-mm diameter; Corning/Costar) were coated overnight at 4°C with soluble elastin (Elastin Products) diluted in PBS (0, 10, 100, or 1000 μg/ml). HUVECs ($\sim 2.5 \times 10^5$ cells/well) were seeded on the elastin-coated transwells in EBM-2-supplemented 20% FBS, 1× glutamine-penicillin-streptomycin, and SingleQuots. After 2 h, the culture medium was replaced, and the number of unattached cells was counted with a hemocytometer to determine plating efficiency. At 14 h after plating, the cells from the upper side of the filter were removed with a cotton swab, and the cells that had migrated through the pores to the opposite side of the membrane were stained with hematoxylin and eosin. The filter was gently cut from the chamber, and the cells that had migrated were counted in 4 high-power fields/insert. For each migration condition, 3 replicates were performed.

Heat treatment of mouse retina

These mouse studies were approved by the Committee on the Ethics of Animal Experiments at the Kyoto Prefectural University of Medicine. C57BL/B6J mice were anesthetized by intraperitoneal injection of 100 mg/kg ketamine and 10 mg/kg xylazine. Pupils were dilated with 1% tropicamide. Heat from an IDL was delivered through a slit lamp (model 30 SL-M; Carl Zeiss Meditec, Oberkochen, Germany) by a trimode IDL emitting at 810 nm (Iris Medical Instrument, Mountain View, CA, USA) at a power setting of 50 mW and a beam diameter of 1.2 mm for 60 s. A series of 4 laser spots were delivered to the posterior pole of each retina at 2 disc diameters from the optic nerve.

To examine the effect of IDL on retinal structure, one IDL spot was delivered to the posterior pole of the retina at 2 disc diameters from the optic nerve. To be able to locate the irradiated spot, a burn was created by argon laser photocoagulation (PC) directly across the optic nerve from the irradiated spot. At 14 d after heat treatment, eyes were enucleated, and the IDL-irradiated retinas were dissected into 0.8-μm sections that were stained with hematoxylin and eosin, and cut into ultrathin sections, which were visualized using a transmission electron microscope.

Induction of CNV in heat-treated mouse retina

At 1 d after the heat treatment, mice were anesthetized as above and fixed on a rack connected to the slit lamp delivery system. To induce CNV, PC burn was placed in the center of the IDL heat treatment area at a power setting of 300 mW and a beam diameter of 50 μm for 0.05 s to induce CNV. Only eyes in which a subretinal bubble was formed following each burn were included in the study. At 7 d after argon photocoagulation, mice were perfused with concanavalin A lectin (20 μg/ml in PBS; Vector Laboratories, Burlingame, CA, USA), then the eyes were enucleated and fixed in 2% paraformaldehyde. The RPE-choroid-sclera complex was flat mounted and was imaged using a Zeiss fluorescence microscope (Univision; Carl Zeiss Meditec). The neovascular area was measured using Scion Image 4.0.2 software (Scion Corp., Frederick, MD, USA).

Statistical analysis

Values are expressed as means ± SE; statistical analysis was performed using the Mann-Whitney U test.

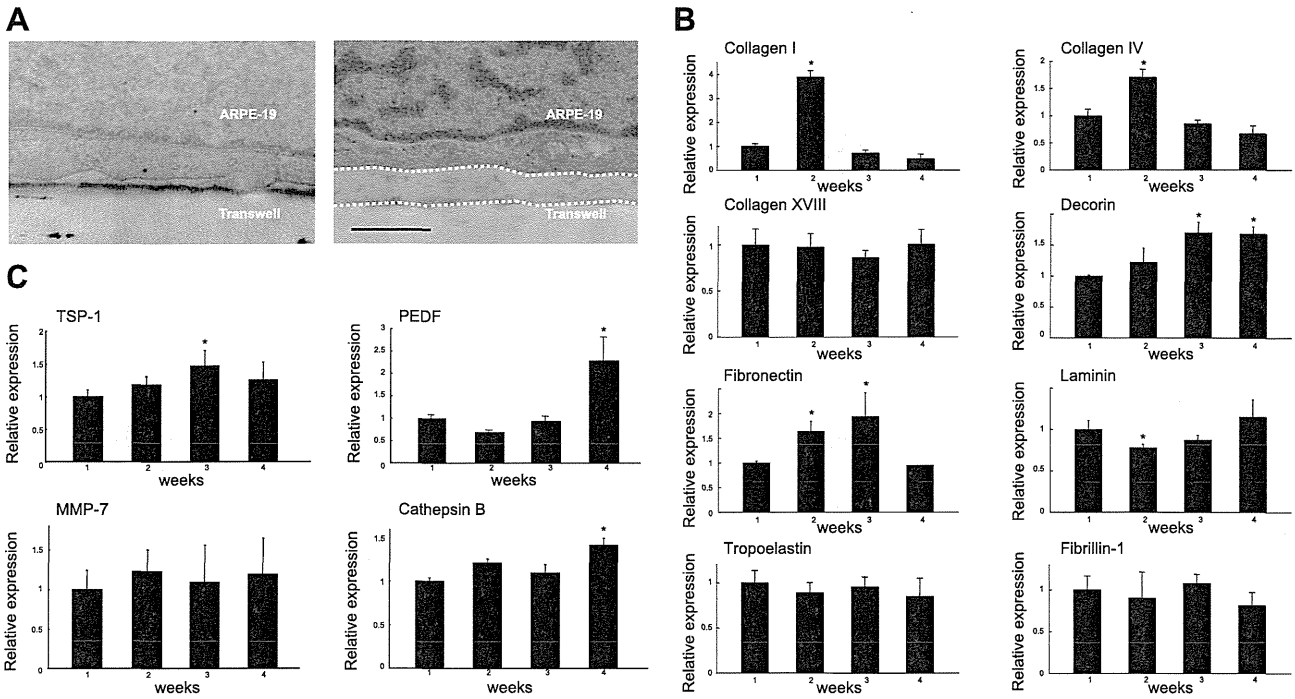

Figure 1. Differentiated ARPE-19 cells secrete components of the BrM. *A*) Transmission electron microscopic examination of ARPE-19 cells after 3 d and 4 wk of culture. Dashed white line shows the accumulation of extracellular matrix under the cells. Scale bar = 0.5 μm. *B*) Real-time PCR analysis of BrM components during ARPE-19 cell differentiation. *C*) Real-time PCR analysis of angiogenesis-related factors during ARPE-19 cell differentiation. Values are expressed as means ± SE (n=3).

RESULTS

ARPE-19 cells secrete a BrM-like matrix

The matrix produced by ARPE-19 cells cultured on transwells for 3 d and 4 wk was examined by transmission electron microscopy. Cells cultured for 3 d had deposited little matrix; however, after culture for 4 wk, a 0.3- to 0.4-μm-thick matrix had accumulated under the basal surface of the cells (**Fig. 1*A***).

ARPE-19 cells cultured for 1, 2, 3, and 4 wk were assessed for the levels of mRNA of the BrM components, including collagen I, collagen IV, collagen XVIII, decorin, fibronectin, laminin, tropoelastin, fibrillin-1, TSP-1, PEDF, MMP-7, and cathepsin B. The expression of collagen IV and I peaked at wk 2, whereas that of decorin began to increase after 2 wk in culture, while that of fibronectin levels were increased at wk 2 and 3. Of the angiogenesis-related proteins, TSP-1 was maximally expressed at wk 3, whereas PEDF and cathepsin B peaked at wk 4. Collagen XVIII, tropoelastin, fibrillin-1, and MMP-7 showed constant expression during the 4 wk of culture (Fig. 1*B*, *C*).

Heat treatment increases ARPE-19 expression of endostatin, TSP-1, and PEDF

Heat treatment at 43°C for 30 min did not affect the viability of the ARPE-19 cells, as detected by TMR red TUNEL labeling (**Fig. 2**). The effect of heat treatment on the levels of TSP-1, PEDF, and endostatin mRNA and protein were examined by real-time PCR and Western blot analysis. TSP-1 mRNA levels were increased significantly at 120 min after heat treatment, and PEDF mRNA levels were elevated significantly as early as 60 min after heat treatment. Collagen XVIII mRNA levels were unchanged after heat treatment, but the mRNA expression of MMP-7, which cleaves the C

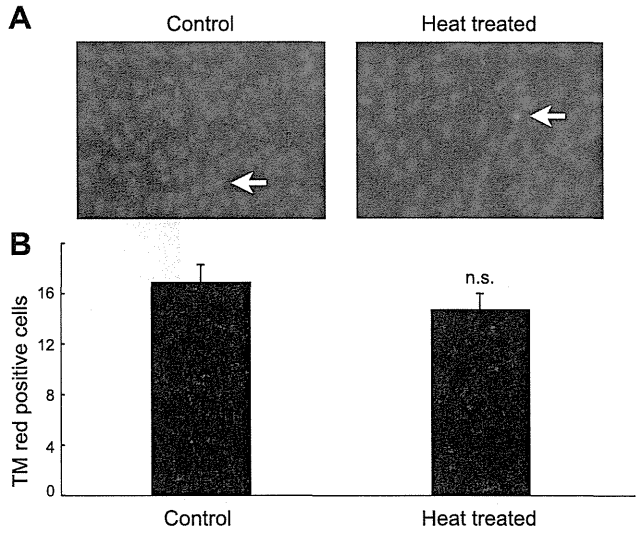

Figure 2. Heat treatment does not affect the viability of ARPE-19 cells. *A*) Representative micrographs of untreated and heat-treated ARPE-19 cells 3 d after heat treatment at 43°C for 30 min. Arrows indicate apoptotic bodies stained with TMR red. *B*) Quantification of the number of apoptotic bodies. Values are expressed as means ± SE. Four random fields were chosen from 3 culture wells.

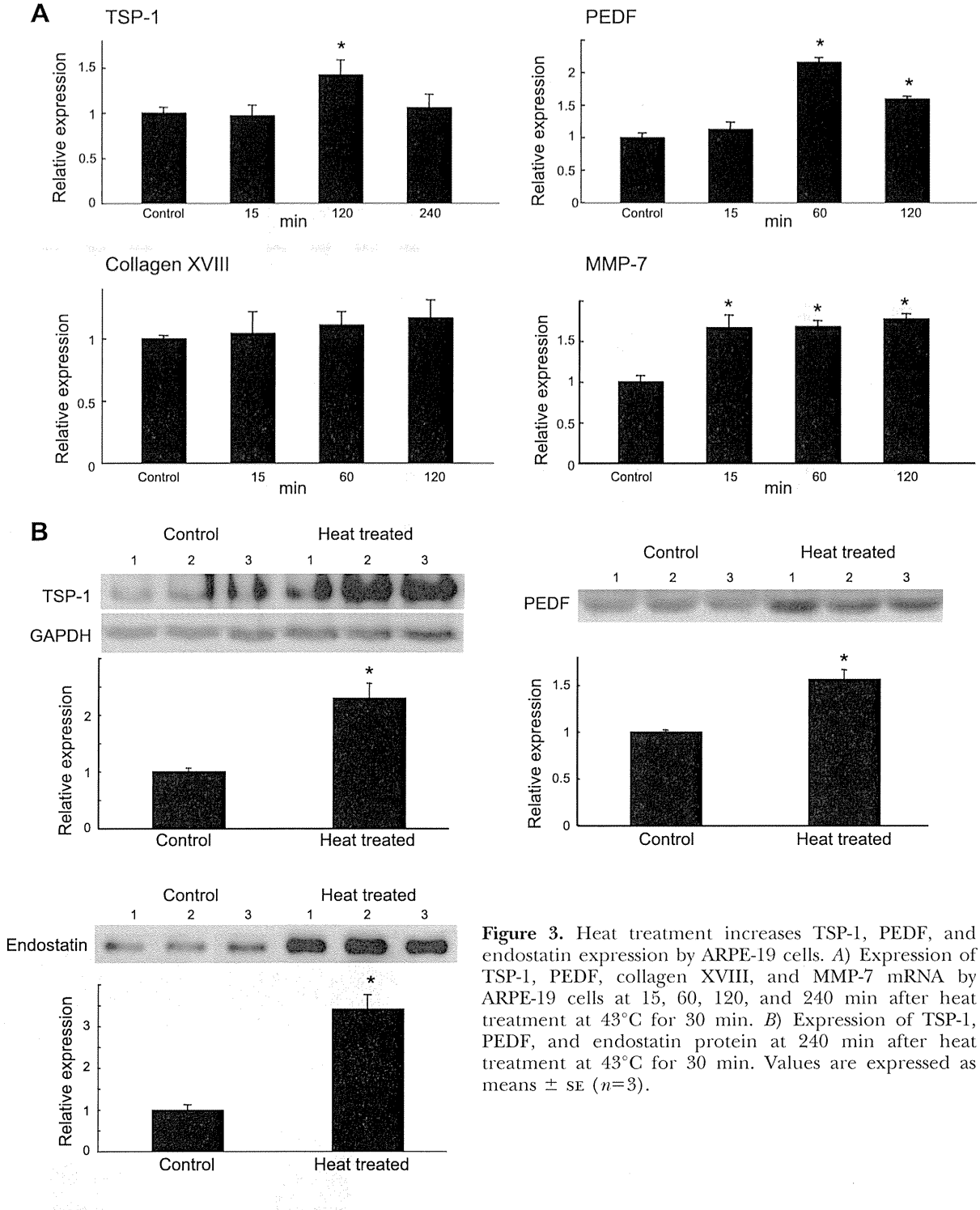

Figure 3. Heat treatment increases TSP-1, PEDF, and endostatin expression by ARPE-19 cells. *A*) Expression of TSP-1, PEDF, collagen XVIII, and MMP-7 mRNA by ARPE-19 cells at 15, 60, 120, and 240 min after heat treatment at 43°C for 30 min. *B*) Expression of TSP-1, PEDF, and endostatin protein at 240 min after heat treatment at 43°C for 30 min. Values are expressed as means ± SE (n=3).

terminus of collagen XVIII to yield endostatin, was increased significantly at 15, 60, and 120 min following heat treatment (**Fig. 3*A***). The levels of cell-associated protein TSP-1 were increased at 240 min after heat treatment, as was the secretion of PEDF and endostatin (Fig. 3*B*).

Heat-treated ARPE-19 cells suppress VEGF-induced corneal angiogenesis

RNA and Western blot analysis indicated that heat treatment of ARPE-19 cells induced an increase in the production of antiangiogenic molecules. To investigate whether heat treatment led ARPE-19 cells to become functionally antiangiogenic, we assayed the effect of heat-treated and control ARPE-19 cells on VEGF-induced angiogenesis using the corneal micropocket assay. The presence of untreated ARPE-19 cells did not affect VEGF-induced corneal angiogenesis; however, the inclusion of heat-treated ARPE-19 cells along with the VEGF pellet in the micropocket led to a nearly 70% reduction in VEGF-induced corneal angiogenesis (**Fig. 4*A***).

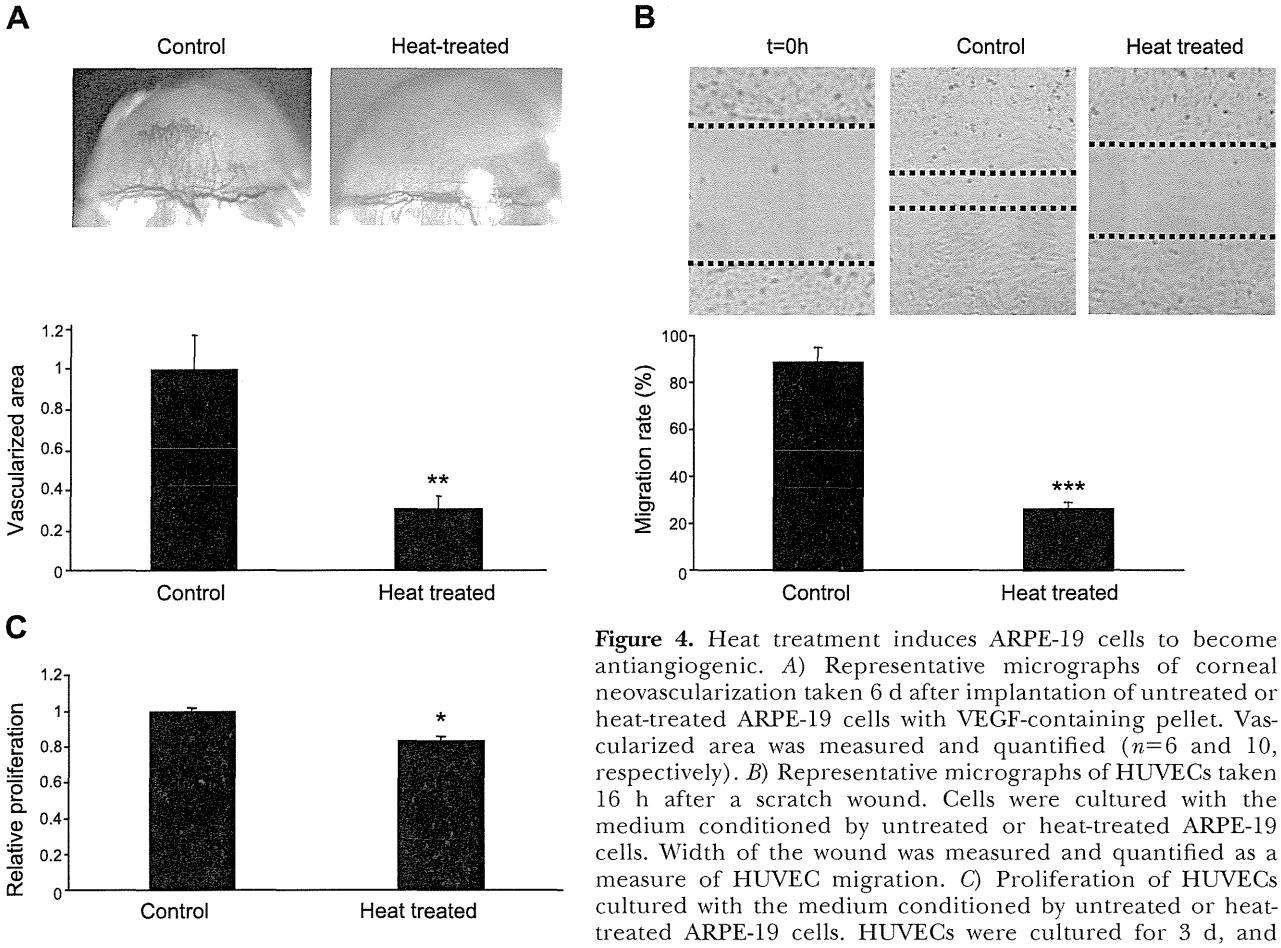

Figure 4. Heat treatment induces ARPE-19 cells to become antiangiogenic. *A*) Representative micrographs of corneal neovascularization taken 6 d after implantation of untreated or heat-treated ARPE-19 cells with VEGF-containing pellet. Vascularized area was measured and quantified (n=6 and 10, respectively). *B*) Representative micrographs of HUVECs taken 16 h after a scratch wound. Cells were cultured with the medium conditioned by untreated or heat-treated ARPE-19 cells. Width of the wound was measured and quantified as a measure of HUVEC migration. *C*) Proliferation of HUVECs cultured with the medium conditioned by untreated or heat-treated ARPE-19 cells. HUVECs were cultured for 3 d, and proliferation was evaluated by direct cell count on trypsin-detached cells with a hemocytometer (n=3). Values are expressed means ± SE.

In the presence of medium conditioned by heat-treated ARPE-19 cells, HUVEC migration and proliferation were suppressed

Incubation of HUVECs in medium conditioned by untreated ARPE-19 cells led the endothelial cells to close almost 90% of a scratch wound in 16 h. In contrast, HUVECs treated with medium conditioned by heat-treated ARPE-19 cells closed just over 25% of the wound (Fig. 4*B*). Treatment of HUVECs with medium conditioned by heat-treated ARPE-19 cells led to a modest but statistically significant reduction in HUVEC proliferation relative to cells treated with medium conditioned by untreated ARPE-19 (Fig. 4*C*).

Heat treatment increased tropoelastin expression by ARPE-19 cells

The effect of heat treatment on the levels of tropoelastin mRNA and protein were examined by real-time PCR and Western blot analysis of cell lysates. Tropoelastin mRNA levels were increased by 180% at 15 min after heat treatment, and the protein levels increased by 170% at 120 min after heat treatment (**Fig. 5*A*, *B***).

Elastin suppressed HUVEC migration in a dose-dependent manner

Elastin coating did not affect the attachment of HUVECs onto the transwells; however, HUVEC migration was reduced by ~20 and 27% when the transwells were coated using 100 and 1000 μg/ml of elastin, respectively (Fig. 5*C*).

Pretreatment with heat reduced the laser-induced CNV

To determine whether pretreatment with heat would affect laser-induced CNV, the retinas of mice were heated by delivering a series of 4 IDL spots to the posterior pole of each retina at 2 disc diameters from the optic nerve, followed by placement of a photocoagulation burn in the center of the heat treatment. Laser-induced CNV was visualized and measured in choroidal flat mounts. The mean size of neovascular areas in heat-treated mice was only 15% that of control mice (**Fig. 6*A***).

To determine whether heat treatment has any effect on normal retina, IDL-irradiated retinal tissues were dissected and examined. The area that had been irradiated by IDL showed no visible structural abnormalities, including atrophic change or fibrosis of neural retina, or recruitment of inflammatory cells (Fig. 6*B*).

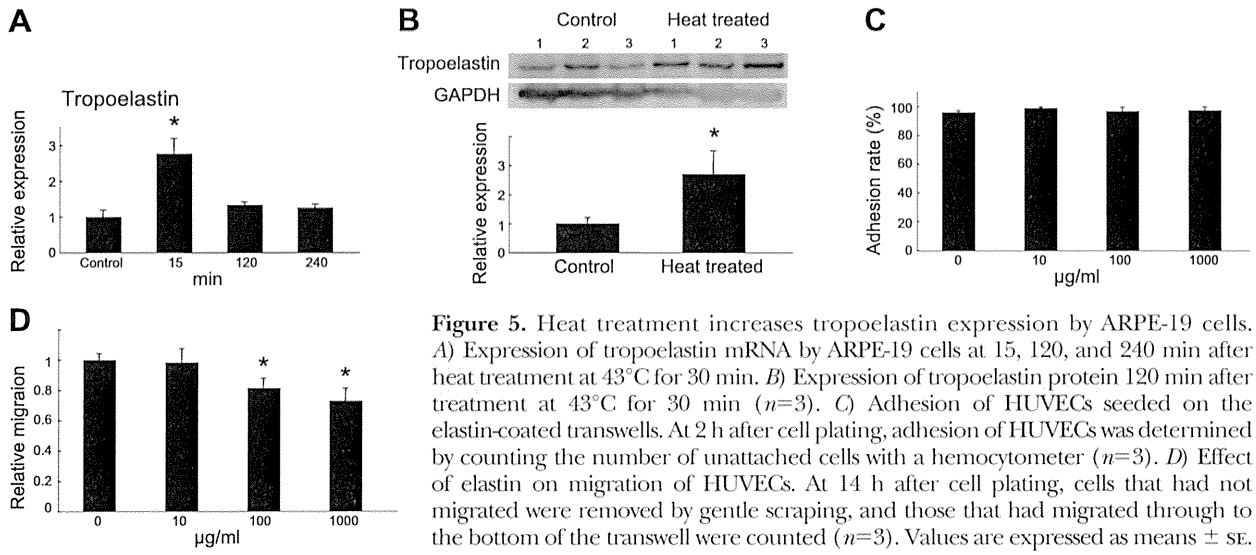

Figure 5. Heat treatment increases tropoelastin expression by ARPE-19 cells. *A*) Expression of tropoelastin mRNA by ARPE-19 cells at 15, 120, and 240 min after heat treatment at 43°C for 30 min. *B*) Expression of tropoelastin protein 120 min after treatment at 43°C for 30 min (n=3). *C*) Adhesion of HUVECs seeded on the elastin-coated transwells. At 2 h after cell plating, adhesion of HUVECs was determined by counting the number of unattached cells with a hemocytometer (n=3). *D*) Effect of elastin on migration of HUVECs. At 14 h after cell plating, cells that had not migrated were removed by gentle scraping, and those that had migrated through to the bottom of the transwell were counted (n=3). Values are expressed as means ± SE.

Transmission electron microscopic examination revealed no change in RPE or photoreceptor cell structure (Fig. 6*C*).

DISCUSSION

In mouse, the BrM begins to develop around d 17 of gestation (15), well after the differentiation of the RPE and the formation of the CC. During the development of BrM, the basement membranes of the RPE and the CC are laid down first, followed by the collagenous layers and finally the inner elastic lamina (15). Studies of human adult BrM reveal no fibroblasts or other cells, except in the extreme periphery (16). These findings suggest that BrM is produced by RPE and/or CC; however, there have been no studies to assess these possibilities.

In this study, we used ARPE-19 cells to determine

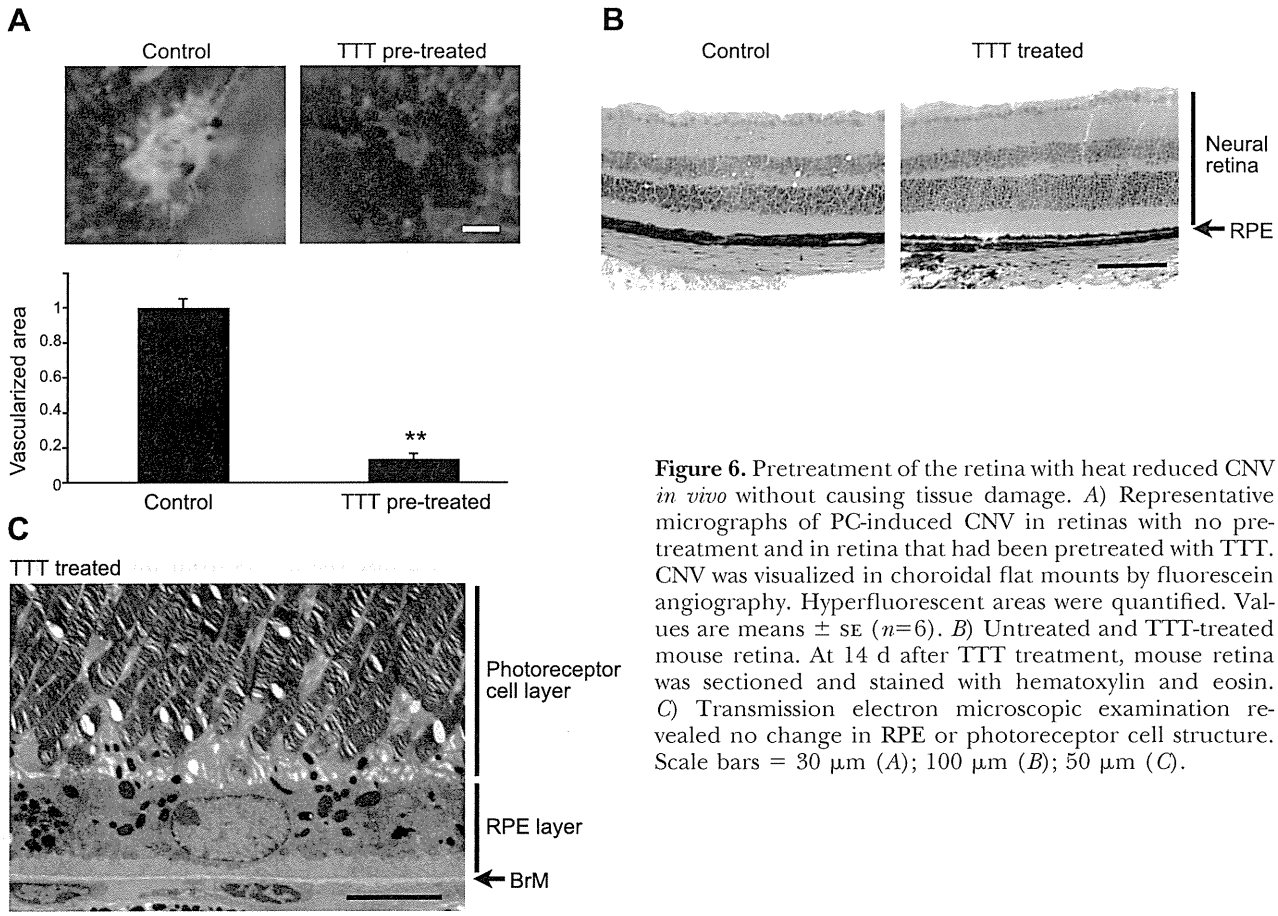

Figure 6. Pretreatment of the retina with heat reduced CNV *in vivo* without causing tissue damage. *A*) Representative micrographs of PC-induced CNV in retinas with no pretreatment and in retina that had been pretreated with TTT. CNV was visualized in choroidal flat mounts by fluorescein angiography. Hyperfluorescent areas were quantified. Values are means ± SE (n=6). *B*) Untreated and TTT-treated mouse retina. At 14 d after TTT treatment, mouse retina was sectioned and stained with hematoxylin and eosin. *C*) Transmission electron microscopic examination revealed no change in RPE or photoreceptor cell structure. Scale bars = 30 μm (*A*); 100 μm (*B*); 50 μm (*C*).

whether RPE can synthesize the various components of BrM. ARPE-19 cells are a well-established line of cells that form differentiated and polarized monolayers after prolonged (4 wk) culture on transwells (17). The apical surface of the ARPE-19 cells represents the retina-facing domain, whereas the basal aspect would be the side that apposes the CC. Using these cells, we have demonstrated that RPE cells produce most of the constituents of BrM and that, after 4 wk in culture, a significant amount of matrix material is deposited basally. Despite the fact that the RPE produces a number of specific BrM components, such as tropoelastin and fibrillin, the matrix that was deposited did not display any structure that would be considered characteristic of pentalaminar BrM. We speculate that the appropriate organization of BrM requires the combined contribution of both the RPE and CC, a notion supported by the recent observation of a lack of a defined BrM in a model of transgenic mice that lack a proper choriocapillaris network (18).

BrM represents both a functional and structural barrier to growth of new blood vessels from the CC into the retinal space. Interestingly, the structure of BrM beneath the macula differs from that under the rest of the retina. Rather than a continuous central elastic layer that is found under most of the retina, the elastic layer under the macula is discontinuous (8). Although this specialization presumably facilitates diffusion of oxygen and nutrients to the metabolically active overlying neural retina, it also renders the macula particularly vulnerable to the development of pathology. The BrM of the patients with early AMD has been documented to contain decreased levels of endostatin, TSP-1, and PEDF (9, 10, 11), as well as fragmentation of the elastic layer (8). A comparison of the BrM proteome profile over the course of AMD revealed decreased levels of collagen I α1 and fibronectin precursor (19). A breach in the structural integrity of BrM is permissive for the formation of new blood vessels. Patients with hypermyopia who present lacquer cracks (breaks in outer retinal layers of macula) frequently develop CNV, and a break in BrM always precedes the development of neovascularization in wet AMD (20). Thus, restoration of the biochemical and structural integrity of BrM could slow or prevent the progression of CNV.

Motivated by observations that heat treatment of skin can induce the production of elastin (12), we investigated the possibility that heat treatment of RPE cells might stimulate their production of BrM components. Incubation of ARPE-19 cells at 43°C for 30 min led to the increased expression of endostatin, TSP-1, PEDF, and tropoelastin mRNA and protein, as well as mRNA levels of collagen I α 1 and fibronectin (data not shown). Cells exposed to high temperatures (44°C for 4 h) develop a transient thermal resistance that protects them by inducing or enhancing the synthesis of a set of HSPs (21). HSP70 and HSP27 have been detected in the RPE, and HSP70 is reported to have an important regulatory role in the protein turnover of human RPE cells (22, 23). Thus, induction of HSP may mediate some of the observed effects of heat on ARPE-19 cells.

Induction of ARPE-19 cells that had been treated with heat blocked VEGF-induced angiogenesis in the corneal pocket assay, whereas the presence of untreated ARPE-19 cells had no effect. Similarly, medium conditioned by heat-treated ARPE-19 cells significantly blocked endothelial cell migration in a wound closure assay. It has been reported that heat-sensitive TRPV channels in RPE increase VEGF secretion (ref). Certainly, incubation of ARPE-19 at 43°C for 30 min led to the increased expression of not only endostatin, TSP-1, and PEDF but also VEGF (data not shown). Although heat treatment of RPE appears to lead to increased expression of both angiogenic- and antiangiogenic factors, the net effect is antiangiogenic. Among the antiangiogenic agents examined, endostatin showed the most prominent heat-induced increase. This observation is consistent with a report that the antiangiogenic effects of endostatin are likely due to its potent inhibition of migration (24).

Motivated by the results of our *in vitro* studies, we tested the effect of heat treatment on new vessel growth in the retina by subjecting the retina to topical heat treatment with IDL. IDL has been previously examined for the treatment of AMD by targeting new vessels as a transpupillary thermotherapy (TTT). Although its safety was proven, and there were some reports of positive effect, results of a multicenter TTT4CNV trial did not show benefit (25). TTT has also been previously used in early AMD with the goal of activating RPE phagocytosis of drusen. However, this approach did not reduce progression to wet AMD (26). The treatment regime used in these prior studies includes 48 shots of TTT with a beam diameter of 125 μm and with power settings of $\geq$50 mW for 0.1 s. The treatment utilized here consisted of 4 applications of laser light (modified TTT) with a beam diameter of 1.2 mm and with power setting of 50 mW for 60 s. Though the previous studies used a similar power level, the spot diameter was 1/10 the size. With a smaller diameter, the energy per unit area increases, very likely destroying the RPE and causing acute inflammation. Such tissue damage does not occur with the treatment protocol employed in our study. In contrast to these early applications where new vessels themselves were targeted and/or very high levels of treatment were applied, our goal was to use pretreatment with heat to restore or increase BrM barrier functions by using mild heat to stimulate RPE cells to produce components of BrM. Our results revealed that pretreatment with heat, or modified TTT, blocked the formation of laser-induced CNV.

Though it is clear that the normal BrM provides a biochemical and physical barrier against CNV, there have been no reports regarding the regeneration of BrM as an approach for increasing its barrier function targeting the management for AMD. Results of our *in vitro* and *in vivo* observations demonstrate that heat treatment may provide a means to restore BrM integrity and its barrier functions against CNV and suggest that

a form of TTT may be used to prevent the development of CNV in patients who are at high risk, such as those with neovascular AMD in a fellow eye. FJ

REFERENCES

1. West, S. K. (2000) Looking forward to 20/20: a focus on the epidemiology of eye diseases. *Epidemiol. Rev.* **22,** 64–70
2. Roth, J. M., Akalu, A., Zelmanovich, A., Policarpio, D., Ng, B., MacDonald, S., Formenti, S., Liebes, L., and Brooks, P. C. (2005) Recombinant alpha2(IV)NC1 domain inhibits tumor cell-extracellular matrix interactions, induces cellular senescence, and inhibits tumor growth in vivo. *Am. J. Pathol.* **166,** 901–911
3. Maeshima, Y., Colorado, P. C., Torre, A., Holthaus, K. A., Grunkemeyer, J. A., Ericksen, M. B., Hopfer, H., Xiao, Y., Stillman, I. E., and Kalluri, R. (2005) Distinct antitumor properties of a type IV collagen domain derived from basement membrane. *J. Biol. Chem.* **275,** 21340–21348
4. Mitola, S., Brenchio, B., Piccinini, M., Tertoolen, L., Zammataro, L., Breier, G., Rinaudo, M. T., den Hertog, J., Arese, M., and Bussolino, F. (2006) Type I collagen limits VEGFR-2 signaling by a SHP2 protein-tyrosine phosphatase-dependent mechanism 1. *Circ. Res.* **98,** 45–54
5. Cockburn, C. G., and Barnes, M. J. (1991) Characterization of thrombospondin binding to collagen (type I) fibres: role of collagen telopeptides. *Matrix* **11,** 168–176
6. Marneros, A. G., She, H., Zambarakji, H., Hashizume, H., Connolly, E. J., Kim, I., Gragoudas, E. S., Miller, J. W., and Olsen, B. R. (2007) Endogenous endostatin inhibits choroidal neovascularization. *FASEB J.* **21,** 3809–3818
7. Yu, H. G., Liu, X., Kiss, S., Connolly, E., Gragoudas, E. S., Michaud, N. A., Bulgakov, O. V., Adamian, M., DeAngelis, M. M., Miller, J. W., Li, T., and Kim, I. K. (2008) Increased choroidal neovascularization following laser induction in mice lacking lysyl oxidase-like 1. *Invest. Ophthalmol. Vis. Sci.* **49,** 2599–2605
8. Chong, N. H., Keonin, J., Luthert, P. J., Frennesson, C. I., Weingeist, D. M., Wolf, R. L., Mullins, R. F., and Hageman, G. S. (2005) Decreased thickness and integrity of the macular elastic layer of Bruch's membrane correspond to the distribution of lesions associated with age-related macular degeneration. *Am. J. Pathol.* **166,** 241–251
9. Bhutto, I. A., Uno, K., Merges, C., Zhang, L., McLeod, D. S., and Lutty, G. A. (2008) Reduction of endogenous angiogenesis inhibitors in Bruch's membrane of the submacular region in eyes with age-related macular degeneration. *Arch. Ophthalmol.* **126,** 670–678
10. Bhutto, I. A., Kim, S. Y., McLeod, D. S., Merges, C., Fukai, N., Olsen, B. R., and Lutty, G. A. (2004) Localization of collagen XVIII and the endostatin portion of collagen XVIII in aged human control eyes and eyes with age-related macular degeneration. *Invest. Ophthalmol. Vis. Sci.* **45,** 1544–1552
11. Uno, K., Bhutto, I. A., McLeod, D. S., Merges, C., and Lutty, G. A. (2006) Impaired expression of thrombospondin-1 in eyes with age related macular degeneration. *Br. J. Ophthalmol.* **90,** 48–54
12. Chen, Z., Seo, J. Y., Kim, Y. K., Lee, S. R., Kim, K. H., Cho, K. H., Eun, H. C., and Chung, J. H. (2005) Heat modulation of tropoelastin, fibrillin-1, and matrix metalloproteinase-12 in human skin in vivo. *Invest. Dermatol.* **124,** 70–78
13. Kang, J. H., Kim, S. A., and Hong, K. J. (2006) Induction of TSP1 gene expression by heat shock is mediated via an increase in mRNA stability. *FASEB J. Lett.* **580,** 510–516
14. Nakao S., Hata Y., Mimura M., Noda K., Kimura Y.N., Kawahara S., Kita T., Hisatomi T., Nakazawa T., Jin Y., Dana M.R., Kuwano M., Ono M., Ishibashi T., and Hafezi-Moghadam, A. (2007) Dexamethasone inhibits interleukin-1β-induced corneal neovascularization: role of nuclear factor-κB-activated stromal cells in inflammatory angiogenesis. *Am. J. Pathol.* **171,** 1058–1065
15. Hirabayashi, Y., Fujimori, O., and Shimizu, S. (2003) Bruch's membrane of the brachymorphic mouse. *Med. Electron. Microsc.* **36,** 139–146
16. Wolter, J. R. (1955) Histologic character of connection between Bruch's membrane and choriocapillaris of human eye; a study with silver carbonate technique. *AMA Arch. Ophthalmol.* **53,** 208–210
17. Dunn, K. C., Aotaki-Keen, A. E., Putkey, F. R., and Hjelmeland, L. M. (1996) ARPE-19, a human retinal pigment epithelial cell line with differentiated properties. *Exp. Eye Res.* **62,** 155–169
18. Marneros, A. G., Fan, J., Yokoyama, Y., Gerber, H. P., Ferrara, N., Crouch, R. K., and Olsen, B. R. (2005) Vascular endothelial growth factor expression in the retinal pigment epithelium is essential for choriocapillaris development and visual function. *Am. J. Pathol.* **167,** 1451–1459
19. School, S., Bode, E., and Tezel, T. H. (2008) Bruch's membrane proteome reveals specific changes in age-related macular degeneration (AMD). *Invest. Ophthalmol. Vis. Sci.* **49,** 1750 (abstr.)
20. Avila, M. P., Weiter, J. J., Jalkh, A. E., Trempe, C. L., Pruett, R. C., and Schepens, C. L. (1984) Natural history of choroidal neovascularization in degenerative myopia. *Ophthalmology* **91,** 1573–1581
21. Landry, J., Chrétien, P., Lambert, H., Hickey, E., and Weber, L. A. (1989) Heat shock resistance conferred by expression of the human HSP27 gene in rodent cells. *J. Cell Biol.* **109,** 7–15
22. Ryhänen, T., Hyttinen, J. M., Kopitz, J., Rilla, K., Kuusisto, E., Mannermaa, E., Viiri, J., Holmberg, C. I., Immonen, I., Meri, S., Parkkinen, J., Eskelinen E. L., Uusitalo, H., Salminen, A., and Kaarniranta, K. (2009) Crosstalk between Hsp70 molecular chaperone, lysosomes and proteasomes in autophagy-mediated proteolysis in human retinal pigment epithelial cells. *J. Cell. Mol. Med.* **13,** 3616–3631
23. Strunnikova, N., Baffi, J., Gonzalez, A., Silk, W., Cousins, S. W., and Csaky, K. G. (2001) Regulated heat shock protein 27 expression in human retinal pigment epithelium. *Invest. Ophthalmol. Vis. Sci.* **42,** 2130–2138
24. Taddei, L., Chiarugi, P., Brogelli, L., Cirri, P., Magnelli, L., Raugei, G., Ziche, M., Granger, H. J., Chiarugi, V., and Ramponi, G. (1999) Inhibitory effect of full-length human endostatin on in vitro angiogenesis. *Biochem. Biophys. Res. Commun.* **263,** 340–345
25. Reichel, E., Musch, D. C., Blodi, B. A., Mainster, M. A., and TTT4CNV Study Group. (2005) Results from the TTT4CNV clinical trial. *Invest Ophthalmol. Vis. Sci.* **46,** 2311 (abstr.)
26. Owens, S. L., Bunce, C., Brannon, A. J., Xing, W., Chisholm, I. H., Gross, M., Guymer, R. H., Holz, F. G., Bird, A. C., and Drusen Laser Study Group. (2006) Prophylactic laser treatment hastens choroidal neovascularization in unilateral age-related maculopathy: final results of the drusen laser study. *Am. J. Ophthalmol.* **141,** 276–281

Received for publication May 31, 2011.
Accepted for publication October 6, 2011.